THE ASTROPHYSICAL JOURNAL, 497:89–107, 1998 April 10

EFFECTS OF INTERACTION-INDUCED ACTIVITIES IN HICKSON COMPACT GROUPS: CO AND FAR-INFRARED STUDY

L. VERDES-MONTENEGRO
Instituto de Astrofísica de Andalucía, CSIC, Apdo. 3004, 18080 Granada, Spain; lourdes@iaa.es
M. S. YUN
National Radio Astronomy Observatory,[1] P.O. Box 0, Socorro, NM 87801; myun@nrao.edu
J. PEREA AND A. DEL OLMO
Instituto de Astrofísica de Andalucía, CSIC, Apdo. 3004, 18080 Granada, Spain; jaime@iaa.es, chony@iaa.es
AND
P. T. P. HO
Harvard-Smithsonian Center for Astrophysics, Cambridge, MA 02138; pho@cfa.harvard.edu
Received 1997 July 7; accepted 1997 November 14

ABSTRACT

A study of 2.6 mm CO $J = 1 \rightarrow 0$ and far-infrared (FIR) emission in a distance-limited ($z < 0.03$) complete sample of Hickson compact group (HCG) galaxies was conducted in order to examine the effects of their unique environment on the interstellar medium of component galaxies and to search for a possible enhancement of star formation and nuclear activity. Ubiquitous tidal interactions in these dense groups would predict enhanced activities among the HCG galaxies compared to isolated galaxies. Instead, their CO and FIR properties (thus, "star formation efficiency") are surprisingly similar to isolated spirals.

The CO data for 80 HCG galaxies presented here (including 10 obtained from the literature) indicate that the spirals globally show the same H_2 content as the isolated comparison sample, although 20% are *deficient* in CO emission. Because of their large optical luminosity, low metallicity is not likely the main cause for the low CO luminosity. The CO deficiency appears linked with the group evolution, and gas exhaustion through past star formation and removal of the external gas reserve by tidal stripping of the outer H I disk offer a possible explanation.

The *IRAS* data for the entire redshift-limited complete sample of 161 HCG galaxies were reanalyzed using ADDSCAN/SCANPI, improving the sensitivity by a factor of 3–5 over the existing Point Source Catalog (PSC) and resolving better the contribution from individual galaxies. The new analysis of the *IRAS* data confirms the previous suggestion that FIR emission in HCG galaxies is similar to isolated, Virgo Cluster, and weakly interacting galaxies. Their H_2 and FIR characteristics yield a star formation efficiency that is similar to that of these comparison samples. A factor 2 enhancement in the 25–100 μm flux ratio among the HCG spirals is found, which suggests intense localized nuclear starburst activity similar to that of H II galaxies.

A number of early-type galaxies in HCGs are detected in CO and FIR, lending further support to the idea that tidal interactions and tidally induced evolution of the groups and member galaxies are important in our sample.

Subject headings: galaxies: abundances — galaxies: clusters: general — infrared: galaxies: — ISM: molecules

1. INTRODUCTION

Hickson (1982) identified 100 compact groups of galaxies by examining Palomar Observatory Sky Survey red plates. A recent complete spectroscopic survey has confirmed that 92 groups have at least three accordant members and 69 groups have at least four true members (Hickson et al. 1992). These compact groups constitute a unique environment to study galaxy interactions because of their high density and low velocity dispersion (300–10^8 h^{-2} Mpc^{-2}, $\langle\sigma\rangle \sim 200$ km s^{-1}; Hickson et al. 1992), which imply a short dynamical lifetime ($\lesssim 10^9$ yr). Members of these groups should experience almost continuous gravitational perturbations and not just encounters, as in the case for pairs (Verdes-Montenegro et al. 1997). Violently interacting galaxies and close pairs show bluer optical colors (Larson & Tinsley 1978), strong far-infrared (FIR) enhancements (Xu & Sulentic 1991; Surace et al. 1993), and higher radio continuum power (Hummel 1981; Hummel et al. 1990) relative to isolated galaxies, and a similar enhancement in star formation and the common occurrence of galaxy mergers are expected among HCG galaxies. However, a rather complex picture emerges from the observations. Zepf, Whitmore, & Levison (1991) and Moles et al. (1994) find from *UBV* photometry that the number of blue ellipticals produced by the merger of spiral galaxies appears to be extremely low. Moles et al. (1994) and Sulentic & Rabaça (1994) concluded, based on optical data, that although star formation is enhanced with respect to isolated galaxies, it is of the same order as in pairs and lower than in violently interacting pairs. Studies of cold gas at the 21 cm line indicate that H I is deficient and frequently disrupted or stripped from individual galaxies or forms a single cloud surrounding the entire group (Williams & van Gorkom 1995 and references therein; Huchtmeier 1997).

Molecular gas is generally thought to be the main ingredient in forming stars and thus of critical importance in

[1] The National Radio Astronomy Observatory is a facility of the National Science Foundation operated under cooperative agreement by Associated Universities, Inc.AU: apdo. OK? spell out?

understanding star-forming activity in galaxies. Enhanced molecular gas content among tidally interacting systems (as measured by the M_{H_2}/L_B ratio) has been suggested by past CO surveys, but we have previously found that the larger M_{H_2}/L_B ratio reported for the bright interacting galaxies in the literature is entirely caused by the nonlinear dependence of M_{H_2}/L_B on L_B, independent of their environment, and that the H_2 content of these systems is at the same level as that of isolated galaxies (Perea et al. 1997). In this paper we report the first major survey of CO $J = 1 \rightarrow 0$ emission among the compact-group galaxies in order to address the impact of their unique environment on their molecular intestellar medium (ISM). The analysis of the CO data suggests that the majority (80%) of the HCG spiral galaxies show a normal level of CO emission, in agreement with a study based on 15 HCG galaxies by Boselli et al. (1996). Among the remaining 20% of the HCG spiral galaxies, a *deficiency* of CO emission is seen, and the CO deficiency appears to be associated with the entire individual groups rather than with odd individual members. The CO emission in two such CO deficient groups, HCG 31 and HCG 92 (Stephan's Quintet), is mapped at high angular resolution using the Owens Valley Millimeter array and found to be highly disturbed (Yun et al. 1997).

We also present a new analysis of the *IRAS* data for our entire distance-limited sample in order to complement the CO study. In an earlier study Hickson et al. (1989b) suggested enhancement of FIR emission among the HCG galaxies based on the analysis of the *IRAS* Point Source Catalog (PSC). However, Sulentic & de Mello Rabaça (1993) and Venugopal (1995) have argued that the same data suggest a normal level of FIR emission if the source confusion is taken into account. The new analysis uses ADDSCAN/SCANPI data, which is 3–5 times more sensitive than the *IRAS* PSC and allows a better resolution of source confusions. *IRAS* HIRES maps are also used to resolve the confusion problem in some cases. Our new analysis finds the FIR luminosity distribution of HCG galaxies to be indistinguishable from that of isolated galaxies and demonstrates that an analysis based on the *IRAS*-detected subsample alone can lead to an erroneous conclusion of FIR enhancement. The suggestion of enhanced nuclear star formation activity based on radio continuum observations by Menon (1995) is supported by the corresponding enhancement in the *IRAS* 25 μm flux.

The organization of the paper is as follows. Our distance-limited complete sample of HCGs, the CO observations of a representative subset, the *IRAS* data analysis, and the details of the comparison samples are discussed in § 2. It is followed by the results of the CO (§ 3) and FIR (§ 4) analyses and the star formation efficiency (§ 5). The interpretation of the CO and FIR analyses are discussed in § 6 in the context of tidal perturbations and other effects in the compact-group environment. The analysis of *IRAS* ADDSCAN/SCANPI data on radio-loud QSOs is utilized to evaluate the formal uncertainties and statistics associated with this data product, and this is discussed separately in the Appendix.

2. OBSERVATIONS AND DATA ANALYSIS

2.1. *Sample Selection and Characteristics*

To conduct the analysis of CO and FIR emission in Hickson compact groups we have selected a statistically complete sample of 39 (out of 100) groups, including 172 galaxies, that satisfy the following criteria:

1. A mean group brightness limit stated to be "complete" by Hickson (1982): $\mu_G \leq 24$ mag arcsec^{-2}.
2. A distance limit to ensure large galaxy angular sizes and less source confusion: $z \leq 0.03$.
3. A minimum membership requirement as determined in Hickson et al. (1992): $N \geq 3$.

Requirements (1) and (2) are complementary and limit the sample to only the nearest groups in which the majority of the members are sufficiently separated for ADDSCAN/SCANPI analysis and CO observations. These criteria also reduce the redshift bias introduced in the original selection of the groups by Hickson (1982), such as the inclusion of poor clusters at high redshifts. Requirement (3) is used to ensure that the selected objects are real physical groups. Spiral and irregular galaxies comprise 56% (89/161) of all galaxies in our complete sample, while the remaining 44% are Es and S0s.

The CO observations presented here include a subset of 80 galaxies (including 10 obtained from the literature; see Table 1) in 24 groups in our complete sample. The groups observed in CO are randomly chosen from our complete sample, in the sense that the groups matched well with the telescope time allocation were observed. A special effort was made to observe every accordant redshift member in each group to avoid any luminosity bias. Nine galaxies in higher redshift groups HCG 35, HCG 85, and HCG 95 ($z \sim 0.03$–0.05) are also observed for a related study, and the results are reported here, but only the low-redshift subsample is included in our statistical analysis. The analysis of the FIR properties is conducted for the entire complete sample for which the *IRAS* observation is available. HCG 42 and HCG 51 fall in the *IRAS* data "gap," and we have obtained ADDSCAN/SCANPI data on the remaining 37 groups (161 galaxies) using the XSCANPI utility.

2.2. *CO Observations*

The CO emission is examined in a total of 70 galaxies in our distance-limited sample plus nine galaxies in the three high-redshift groups HCG 35, HCG 85, and HCG 95 ($z \sim 0.03$–0.05). The majority (74/79) are observed with the NRAO 12 m telescope at Kitt Peak during three separate observing sessions between 1995 October and 1996 October, and two galaxies are observed using the 37 m radio telescope at Haystack Observatory[2] in January 1996. Both telescopes were equipped with SIS receivers, with typical system temperatures of 300–500 K (single-sideband) and 600–900 K (single-sideband), respectively. The beam sizes at 115 GHz are 55″ and 18″ (FWHM). The 500 MHz filter banks at 2 MHz resolution and the 600 MHz hybrid digital spectrometer with 0.78 MHz resolution were used to record the NRAO 12 m telescope data, and a 320 MHz autocorrelation spectrometer at 1.25 MHz resolution was used for the Haystack observations. In addition, ^{12}CO ($J = 2 \rightarrow 1$) observations of three galaxies in HCG 61 were obtained at the Caltech Submillimeter Observatory[3] 10.4 m

[2] Radio Astronomy at Haystack Observatory of the Northeast Radio Observatory Corporation is supported by the National Science Foundation

[3] The Caltech Submillimeter Observatory is funded by the National Science Foundation under contract AST-9313929.

TABLE 1

OBSERVED AND DERIVED CO PROPERTIES

HCG Galaxy[a]	Type[b]	R_{25}[c] (arcsec)	Beam (arcsec)	v_{opt}[d] (km s^{-1})	v_{CO}[e] (km s^{-1})	T_{mb}[f] (mK)	Δv_{CO}[g] (km s^{-1})	I_{CO}[h] (K km s^{-1})	M_{H_2} (10^8 $M_\odot$)	log L_B ($L_\odot$)	Other Names
HCG 7b	SB0	40.1	55	4238	...	...	...	<0.7	<7.3	10.18	N196
HCG 7c	SBc	52.3	55	4366	4422	18.1	183	1.4	15.0	10.65	N201
HCG 10a	SBb	104.8	55	5148	...	...	...	<0.9	<10.7	10.79	N536
HCG 10b	E1	51.2	55	4862	...	...	...	<0.9	<12.5	10.72	N529
HCG 10c	Sc	55.4	55	4660	...	...	...	<0.9	<12.1	10.12	N531
HCG 10d	Scd	29.2	55	4620	...	...	...	<1.6	<22.0	9.86	N542
HCG 18b	S/Irr	50.0	55	4082	4059	7.3	42	0.6	6.2	9.66	U2140a
HCG 18c	Im	22.8	55	4143	...	...	...	<0.3	<3.1	9.39	U2140b
HCG 21a	Sc	44.8	55	7614	7618	15.2	555	4.8	165.6	10.53	...
HCG 21b	Sab	45.9	55	7568	...	...	...	<0.6	<21.8	10.65	...
HCG 21c	E1	29.2	55	7356	...	...	...	<0.8	<26.6	10.54	...
HCG 21d	E2	18.0	55	8835	...	...	...	<0.8	<29.0	10.27	...
HCG 21e	SB0a	17.4	55	8843	...	...	...	<0.9	<30.8	10.02	...
HCG 22a	E2	79.8	55	2705	...	...	...	<0.7	<3.0	10.38	N1199
HCG 22b	Sa	30.6	55	2625	...	...	...	<0.8	<3.6	9.46	...
HCG 22c	SBcd	52.3	55	2728	...	...	...	<1.0	<4.0	9.71	...
HCG 30a	SBa	55.5	55	4697	...	...	...	<0.7	<9.2	10.62	...
HCG 30b	Sa	36.5	55	4625	...	...	...	<0.7	<9.1	10.29	...
HCG 30c	SBbc	17.3	55	4508	...	...	...	<0.8	<9.7	9.69	...
HCG 30d	S0	15.4	55	4666	...	...	...	<0.8	<10.9	9.49	...
HCG 31a	Sdm	32.3	55	4042	3999[i]	8.0[i]	168[i]	0.4[j]	4.4[j]	9.69	N1741
HCG 31c	Im	18.3	55	4068						10.62	M1089
HCG 31b[j]	Sm	26.1	55	4171	...	...	...	<0.7	<7.2	9.92	...
HCG 31g[k]	Irr	18.0	55	4012	...	...	...	<0.4	<4.1	9.73	M1090
HCG 33a	E1	11.1	55	7570	...	...	...	<0.5	<17.1	10.05	...
HCG 33c	Sd	23.3	55	7823	7809	7.9	196	1.0	38.2	9.64	...
HCG 35a	S0	14.4	55	15919	...	...	...	<0.3	< 43.5	9.75	...
HCG 35d	Sc	11.6	55	15798	...	...	...	<0.3	< 51.6	9.22	...
HCG 35f	E1	4.1	55	16330	...	...	...	<0.3	< 51.6	8.79	...
HCG 38a	Sbc	22.1	55	8760	8662	9.8	362	1.4	67.3	10.21	...
HCG 38b	SBd	30.0	55	8739	8691[i]	9.6[i]	258[i]	1.4[i]	66.4[i]	10.39	U5044a
HCG 38c	Im	21.8	55	8770						10.10	U5044b
HCG 44a	Sa	100.7	18	1293	...	...	...	<20.7	<2.6	10.02	N3190
HCG 44c	E2	56.8	18	1218	...	...	...	<16.5	<2.0	9.55	N3185
HCG 48a	E2	45.7	55	3014	...	...	...	<1.0	<4.8	9.84	I2597
HCG 48b	Sc	22.0	55	2385	...	...	...	<1.2	<5.9	9.32	...
HCG 48c	S0a	15.4	55	4203	4266	13.5	329	1.6	7.7	9.38	...
HCG 48d	E1	8.8	55	3045	2969	12.1	111	0.9	4.1	8.71	...
HCG 59a	Sa	17.7	55	4109	4122	14.9	57	1.0	10.2	9.84	I736
HCG 59b	E0	15.0	55	3908	...	...	...	<0.9	<8.8	9.52	...
HCG 59c	Sc	24.7	55	4347	...	...	...	<0.7	<7.2	9.92	...
HCG 59d	Im	17.7	55	3866	...	...	...	<0.7	<6.6	9.25	I737
HCG 61a	E/S0	54.3	30	3784	3683	12.9	84	0.6	1.7	10.45	N4169
HCG 61c	Sbc	51.8	30	3956	3950	39.4	561	10.3	28.2	10.19	N4175
HCG 61d	S0	25.6	30	3980	...	...	...	<0.7	<1.9	9.97	N4174
HCG 67a	E1	58.8	55	7262	...	...	...	<0.9	<28.0	11.07	...
HCG 67b	Sc	68.4	55	7644	7625	8.8	234	2.3	75.3	10.63	...
HCG 67c	Scd	19.9	55	7430	...	...	...	<0.8	<25.6	10.13	...
HCG 68a	S0	77.4	55	2162	1840	18.1	485	2.1	7.4	10.40	N5353
HCG 68b	E2	86.4	55	2635	...	...	...	<0.7	<2.1	10.36	N5354
HCG 68c	SBbc	76.7	55	2313	2336	25.2	327	5.1	17.8	10.36	N5350
HCG 68d	E3	31.1	55	2408	2535	11.1	50	0.3	1.2	9.68	N5355
HCG 69a	Sc	47.5	55	8856	...	...	...	<0.7	<30.8	10.34	U8842
HCG 69b	SBb	14.8	55	8707	...	...	...	<0.6	<34.1	10.07	...
HCG 69c	S0	13.4	55	8546	...	...	...	<0.7	<26.6	10.34	U8842
HCG 69d	SB0	10.8	55	9149	...	...	...	<0.7	<30.8	9.95	U8842
HCG 79b	S0	60.5	55	4446	...	...	...	<0.5	<5.8	10.21	N6027
HCG 79c	S0	40.3	55	4146	...	...	...	<0.5	<5.8	9.77	N6027
HCG 85a	E1	16.0	55	11155	...	...	...	<0.3	<26.3	8.48	...
HCG 85b	E1	13.1	55	12122	...	...	...	<0.3	<24.6	8.81	...
HCG 88b	SBb	34.0	55	6010	...	...	...	<0.8	<17.9	10.68	N7977
HCG 88c	Sc	27.6	55	6083	5952	17.6	251	2.0	44.3	10.43	N6976
HCG 88d	Sc	32.7	55	6032	...	...	...	<1.0	<21.7	10.18	N6975
HCG 90a	Sa	71.8	55	2575	2495	18.1	586	6.0	25.7	10.29	N7172
HCG 90b	E0	39.9	55	2525	2762[i]	18.3[i]	618[i]	5.8[i]	24.8[i]	10.19	N7176
HCG 90d	Im	69.3	55	2778						10.16	N7174
HCG 90c	E0	36.6	55	2696	2651	19.2	18	0.7	3.0	10.12	N7173
HCG 92a	Sd	69.8	55	786	780	20.7	22	0.3	0.1	9.17	N7320
HCG 92b	Sbc	66.6	55	5774	...	...	...	<0.5	<12.6	10.66	N7318B
HCG 92c	SBc	52.8	55	6764	6657	6.1	195	0.6	15.1	10.74	N7319
HCG 92d	Sc	36.6	55	6630	...	...	...	<0.5	<15.1	10.60	N7318A
HCG 95a	E3	26.3	55	11888	...	...	...	<0.4	<30.1	10.86	N7609

TABLE 1—*Continued*

HCG Galaxy[a]	Type[b]	R_{25}[c] (arcsec)	Beam (arcsec)	v_{opt}[d] (km s^{-1})	v_{CO}[e] (km s^{-1})	T_{mb}[f] (mK)	Δv_{CO}[g] (km s^{-1})	I_{CO}[h] (K km s^{-1})	M_{H_2} (10^8 $M_\odot$)	log L_B ($L_\odot$)	Other Names
HCG 95b	Scd	20.7	55	11637	...	...	...	<0.3	<25.8	10.42	...
HCG 95c	Sm	28.4	55	11562	...	...	...	<0.4	<30.1	10.46	...
HCG 95d	Sc	22.1	55	12350	...	...	...	<0.4	<31.0	10.16	...
HCG 96a	SBc	33.3	55	8670	8664	31.8	251	5.1	239.9	10.90	N7674
HCG 96b	E2	18.7	55	8585	...	...	...	<0.3	<14.1	10.53	N7675
HCG 96c	Sa	12.2	55	8805	8912	5.7	92	0.4	18.6	10.05	...
HCG 96d	Sm	6.6	55	9025	...	...	...	<0.8	<37.2	9.69	...
I 883	S+S	46.5	55	6892	6996	26.8	476	7.2	208.4	10.40	...
N 2738	S?	43.4	55	3065	3120	33.3	230	3.4	19.5	10.07	...
N 6090	S+S	50.9	55	8785	8824	41.7	130	4.3	202.1	...	...
Data from Bibliography											
HCG 7a[l]	Sb	56.8	43	4210	4168	...	500	7.2	49.2	10.47	N192
HCG 7d[l]	SBc	38.3	43	4116	...	...	...	<0.6	<2.5	9.73	N197
HCG 16a[l]	SBab	34.9	43	4152	4061	...	370	8.7	51.3	10.55	N835
HCG 16b[l]	Sab	49.4	43	3977	3786	...	560	2.3	13.5	10.30	N833
HCG 16c[l]	Im	31.5	43	3861	3829	...	270	9.2	53.7	10.34	N838
HCG 16d[l]	Im	41.1	43	3847	3846	...	240	6.5	38.0	10.21	N839
HCG 37a[m]	E7	51.9	23	6745	...	...	...	<1.4	<6.6	10.91	N2783
HCG 44d[n]	Sd	67.7	23	1579	1550	40	60	3.0	0.6	9.56	N3187
HCG 87a[l]	Sbc	39.8	43	8694	...	...	...	<0.5	<14.8	10.71	...
HCG 88a[l]	Sb	45.1	43	6033	...	...	...	1.2	16.2	10.71	N6978

[a] Notation as in Hickson et al. 1992.
[b] Morphological types from Mendes de Oliveira & Hickson 1994 and Williams & Rood 1987. In the case of H61a, although classified by Mendes de Oliveira & Hickson 1994 as S0a, Rubin et al. 1991 indicate that it is an elliptical galaxy, according to its light profile.
[c] Radius in arcseconds of the $\mu_B = 25.0$ mag arcsec^{-2} isophote from Hickson 1993.
[d] Optical velocities from Hickson 1993, except for H18b from Williams & van Gorkom 1988, and H96 from our optical spectroscopy data (Verdes-Montenegro et al. 1997).
[e] Intensity-weighted velocity in the range for which the line has been detected.
[f] Peak-line main-beam brightness temperature in units of millikelvins.
[g] Full width of the CO line measured at a 30% of the peak line temperature given in column (6), except for galaxies from Boselli et al. 1996, for which the corresponding level is not given.
[h] Given fluxes are already corrected for extended sources, as explained in § 2.3. Upper limits for nondetection have been calculated by taking the 3 σ rms noise multiplied by an assumed line width of 300 km s^{-1}and divided by the square root of number of channels in that velocity range.
[i] The emission is unresolved. Therefore we give parameters for the global profile.
[j] The upper limits is from Kitt Peak observations, and the lower one from OVRO measurement (Yun et al. 1997) sensible to the more compact emission.
[k] This member has been added to H31 by Rubin et al. 1990.
[l] Data from Boselli et al. 1996.
[m] Data from Wiklind et al. 1995.
[n] Data from Braine & Combes 1993.

telescope at Mauna Kea, Hawaii, in 1996 April. The facility SIS receiver with typical system temperature of 400 K (single-sideband) was used with a 1024 channel 1.5 GHz acousto-optical spectrometer, and the beam size at 230 GHz was about 30″.

The observed positions correspond either to the radio continuum source locations reported by Menon (1995) and Menon & Hickson (1985) when available or to the optical positions given by Hickson (1993). Pointing was checked frequently by observing nearby planets or quasars, and the rms pointing uncertainty of the telescopes was better than 3″–5″ in all cases. All observations were made using the beam switching mode with a typical beam throw of 3′ at ~1 Hz frequency, and resulting flat and well-behaved spectra required only linear baseline removal in most cases. For the analysis two polarization spectra are averaged and Hanning smoothed to 15–20 km s^{-1} velocity resolution in order to improve the signal-to-noise ratio. The CO spectra of the detected galaxies are shown in Figure 1, including those of IC 883, NGC 2738, and NGC 6090 that were taken for system tests. The CO spectrum in NGC 2738 has never been reported previously, but its bright CO line is not surprising, given its bright 60 μm flux.

Out of 80 galaxies observed, CO emission is detected in 28 resolved galaxies and in three unresolved pairs. Good upper limits are obtained for the remaining 48 galaxies and the high-redshift group galaxies. The detection rate is 50% for spiral galaxies and 20% for early-type galaxies. The observed and derived quantities, such as CO central velocity (col. [6]), brightness temperatures in the main-beam scale (col. [7]), line width (col. [8]), and CO integrated intensity (col. [9]) are listed in Table 1. The optical size of the galaxies is larger than the observed beam in 15 cases, and ~10% correction to the total fluxes is made assuming an exponential distribution for gas (see Young et al. 1995). Because most published CO surveys are biased toward IR or optically luminous isolated spirals, CO data is reported on only 14 HCG galaxies in the literature. Four galaxies (H7c, H90a, H90b, and H90d) are observed again to confirm our NRAO 12 m observations, and the correction technique for the small observing beam has produced consistent results with the published measurements.

2.3. *ADDSCAN/SCANPI Analysis of the IRAS Data*

By definition, Hickson compact groups consist of several galaxies located within a diameter region of a few arcminutes, and the differentiating contribution from individual galaxies is difficult in the *IRAS* full-resolution data (angular

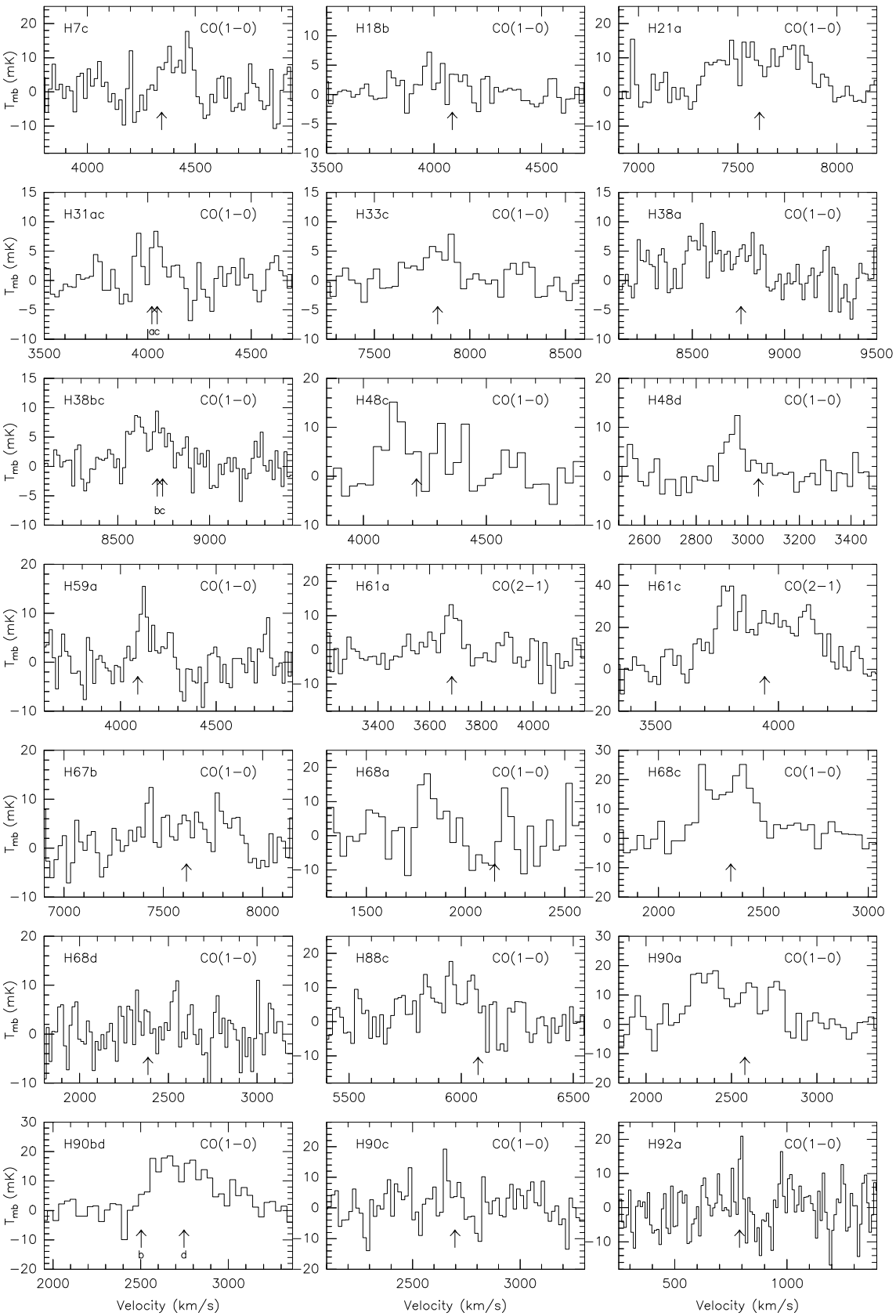

FIG. 1.—CO spectra of the 21 galaxies and three unresolved pairs that are detected. Five galaxies from our HCG sample have been detected by other authors (H7a and all four members of HCG 16 were detected by Boselli et al. 1996) and are not shown here. The optical velocities of each galaxy are marked with an arrow. The CO spectra of IC 883, NGC 2738, and NGC 6090, observed for system tests, are also shown.

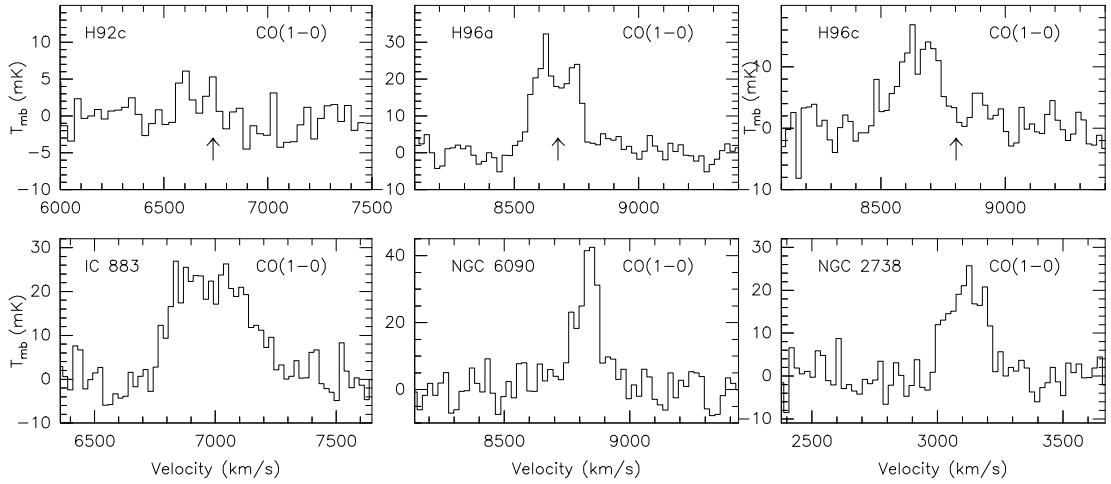

FIG. 1—*Continued*

resolution $\sim 4'$ at 100 μm). In an earlier study Hickson et al. (1989b) suggested enhancement of FIR emission among HCG galaxies based on the analysis of *IRAS* PSC data. However, Sulentic & de Mello Rabaça (1993) and Venugopal (1995) argued that the same data suggest a normal level of FIR emission if the presence of two or more IR sources in several unresolved HCGs are taken into account. Two extra steps are taken here to improve the analysis of the IR properties of HCG galaxies: (1) obtaining higher spatial resolution information with improved sensitivity using *IRAS* ADDSCAN/SCANPI data, and (2) limiting our statistical analysis to a complete sample of nearby ($z \leq 0.03$) groups only and minimizing the luminosity bias.

ADDSCAN/SCANPI is a one-dimensional co-adder of the calibrated *IRAS* survey data available at the Infrared Processing and Analysis Center. It performs co-addition of all scans that passed over a specific position in the *IRAS* raw survey data and produces a scan spectrum along the average scan direction with flux scaling accurate to a few percent of PSC. While the intrinsic resolution of ADDSCAN/SCANPI is about $1'$ at the 60 μ band, the centroid of the source can be determined with much higher accuracy ($1\ \sigma \sim 7''$ for S/N > 5; see Appendix; Surace et al. 1993). Furthermore, ADDSCAN/SCANPI data is about 3–5 times more sensitive than *IRAS* PSC, and we were able to achieve detections of fainter *IRAS* sources and place better upper limits on undetected sources. The results of ADDSCAN/SCANPI analysis of the 12, 25, 60, and 100 μm bands for 161 galaxies in 37 HCGs are given in Table 2. For several compact groups with a high degree of confusion (e.g., HCG 33, HCG 40, HCG 56, and HCG 88), 60 μm HIRES maps are obtained to identify the IR sources.

Among the distance-limited complete sample of 39 HCGs, all but one group (HCG 46) have at least one galaxy detected in our XSCANPI analysis, while no *IRAS* data is available for two groups (HCG 42 and HCG 51). At least 67 and 61 out of 161 galaxies are detected at the 60 and 100 μm bands, respectively, including five unresolved pairs (HCG 31ac, HCG 38bc, HCG 90bd, HCG 91ad, and HCG 96ac) and one unresolved quartet (HCG 54). The comparison of our results with the HIRAS analysis of HCG galaxies by Allam et al. (1996) clearly demonstrates that the ADDSCAN/SCANPI process is more sensitive for detection than the HIRAS process—this is expected, since HIRAS and other methods using a maximum likelihood estimator require a high S/N. For example, among the same 36 groups for which we report at least one *IRAS* detection, Allam et al. report nondetection in eight groups (HCG 22, HCG 30, HCG 62, HCG 86, HCG 87, HCG 97, HCG 98, and HCG 99). Among 91 commonly resolved galaxies, the total number of detections reported in our/their data at 12, 25, 60, and 100 μm are 30/11, 29/15, 44/37, and 39/33, respectively. On the other hand, the accuracy of the flux determination is mutually verified, since the difference between the measured fluxes for the commonly detected galaxies has a zero median and is nearly always within 2 σ of the median.

2.4. *Comparison Samples*

In order to investigate whether the observed CO and FIR characteristics of HCG galaxies show any observable effects of being subjected to continuous tidal disruptions in a compact-group environment, comparison samples of isolated and interacting galaxies are constructed, matching absolute-magnitude distribution whenever possible. For the CO study, we have compiled from the literature an extensive comparison sample of 207 galaxies of varying interaction classes and environments, representing a wide range of luminosity ($10^{8.6}\ L_\odot < L_B < 10^{11.4}\ L_\odot$) and for which FIR, CO, and B luminosity are available. Because many nearby galaxies typically subtend several arcminutes in size and are much larger than the beams of the telescopes, the comparison data consist mostly of CO surveys using at least partial mapping (e.g., Young et al. 1995). The "isolated" galaxy sample consists of 68 objects compiled from the distance-limited survey of the Nearby Galaxies Catalog (Tully 1988) by Sage (1993) and interaction class 0 objects of the Solomon & Sage survey (1988, hereafter SS88). Morphological types range from Sa to Sd, with $10^{8.6}\ L_\odot \geq L_B \geq 10^{10.9}\ L_\odot$. This sample lacks completeness, because CO surveys found in the literature are frequently biased toward infrared-luminous galaxies, but a wide range of luminosity represented allows us to characterize the CO emission in the isolated environment. Only upper limits are available for six galaxies. The "weakly perturbed" (WP) galaxy sample consists of 43 galaxies including interaction

TABLE 2

FIR Parameters of Our Sample of HCG Galaxies

Galaxy	I_{12} (Jy)	I_{25} (Jy)	I_{60} (Jy)	I_{100} (Jy)	L_{FIR} ($L_\odot$)
HCG 3a	<0.132	<0.141	0.240	<0.336	<9.558
HCG 3b	<0.099	<0.114	<0.176	<0.528	<9.634
HCG 3c	<0.126	<0.147	0.640	1.200	10.433
HCG 3d	<0.111	<0.120	0.150	<0.384	<9.523
HCG 4a	0.300	0.650	4.230	8.880	10.957
HCG 4b	<0.117	<0.105	0.400	<0.300	<9.673
HCG 4c	<0.056	<0.108	<0.090	<0.306	<9.478
HCG 4d	<0.111	<0.114	<0.117	<0.297	<9.458
HCG 4e	<0.093	<0.111	<0.087	<0.351	<10.152
HCG 7a	0.230	0.370	3.320	6.610	10.2787
HCG 7b	<0.099	<0.225	<0.183	<0.318	<9.001
HCG 7c	0.180	0.310	0.610	2.350	9.722
HCG 7d	<0.114	<0.210	<0.153	<0.390	<8.972
HCG 10a	<0.069	0.120	0.500	1.810	9.764
HCG 10b	<0.075	<0.078	<0.108	0.470	<9.097
HCG 10c	0.090	<0.201	0.780	2.060	9.795
HCG 10d	<0.084	<0.108	<0.120	<0.276	<8.946
HCG 16a	0.350	0.400	5.730	12.830	10.526
HCG 16b	<0.06	<0.100	<0.120	<0.330	<8.822
HCG 16c	1.100	2.060	12.200	19.990	10.731
HCG 16d	0.500	2.400	11.800	12.000	10.6465
HCG 18a	<0.108	<0.117	<0.108	<0.300	<9.617
HCG 18b	<0.090	<0.096	<0.129	<0.357	<8.909
HCG 18c	<0.096	<0.117	<0.105	<0.357	<8.881
HCG 18d	<0.102	0.140	0.530	1.610	9.541
HCG 21a	0.190	0.170	1.040	3.200	10.384
HCG 21b	<0.063	<0.111	0.240	1.350	9.903
HCG 21c	<0.090	<0.096	<0.099	<0.306	<9.333
HCG 21d	<0.090	<0.111	<0.147	<0.492	<9.6841
HCG 21e	<0.090	<0.111	0.180	0.440	9.7011
HCG 22a	0.060	<0.093	0.100	<0.363	<8.505
HCG 22b	<0.075	<0.063	<0.174	<0.282	<8.5493
HCG 22c	<0.069	<0.081	0.250	0.810	8.882
HCG 22d	<0.057	<0.099	<0.156	<0.384	<9.689
HCG 22e	<0.075	<0.084	<0.159	<0.432	<9.739
HCG 30a	<0.144	<0.087	<0.090	0.550	<9.086
HCG 30b	<0.084	<0.090	0.100	<0.438	<9.022
HCG 30c	<0.105	0.140	0.170	0.750	9.2322
HCG 30d	<0.069	<0.069	<0.096	<0.297	<8.923
HCG 31ac	0.130	0.750	4.980	6.690	10.365
HCG 31b	0.078	0.060	0.081	0.384	8.862
HCG 31d	<0.072	<0.051	<0.087	<0.387	<10.510
HCG 31g	<0.090	<0.075	0.500	0.400	9.283
HCG 33a	0.078	<0.102	<0.114	<1.900	<9.938
HCG 33b	<0.078	<0.126	<0.165	<2.073	<10.039
HCG 33c	0.130	0.240	0.680	1.840	10.193
HCG 33d	<0.096	<0.132	0.500	<2.400	<10.199
HCG 37a	0.220	<0.093	0.560	2.300	10.082
HCG 37b	0.200	0.290	0.660	2.130	10.091
HCG 37c	<0.096	<0.111	<0.093	<0.261	<9.284
HCG 37d	<0.090	<0.105	<0.081	<0.123	<8.957
HCG 37e	<0.086	<0.135	<0.108	<0.165	<9.104
HCG 38a	<0.069	<0.189	0.440	1.200	10.105
HCG 38bc	0.100	0.270	1.600	3.370	10.611
HCG 38d	<0.102	0.180	0.190	<0.600	<10.670
HCG 40a	<0.060	<0.084	<0.099	<0.300	<9.238
HCG 40b	<0.057	<0.093	<0.084	<0.255	<9.905
HCG 40c	0.090	0.110	0.850	2.000	10.149
HCG 40d	<0.072	0.100	1.030	2.300	10.170
HCG 40e	<0.066	<0.090	<0.099	<0.240	<9.188
HCG 42			IRAS GAP		
HCG 44a	0.350	0.460	3.400	10.72	9.359
HCG 44b	<0.084	<0.129	<0.123	<0.390	<7.975
HCG 44c	0.210	0.280	1.550	3.710	8.905
HCG 44d	<0.099	0.240	1.300	3.120	9.055
HCG 46a	<0.060	<0.204	<0.066	<0.210	<9.259
HCG 46b	<0.081	<0.120	<0.066	<0.210	<9.298
HCG 46c	<0.081	<0.114	<0.090	<0.219	<9.301
HCG 46d	<0.090	<0.123	<0.075	<0.219	<9.240
HCG 48a	0.430	<0.111	<0.102	<0.429	<8.398
HCG 48b	0.160	0.320	0.960	2.150	9.286
HCG 48c	<0.066	<0.102	<0.090	<0.183	<8.748

TABLE 2—*Continued*

Galaxy	I_{12} (Jy)	I_{25} (Jy)	I_{60} (Jy)	I_{100} (Jy)	L_{FIR} ($L_\odot$)
HCG 48d	<0.057	<0.084	<0.093	<0.141	<8.404
HCG 51			IRAS GAP		
HCG 54[a]	<0.051	0.240	0.500	0.840	8.465
HCG 56a	<0.060	<0.069	<0.111	<0.371	<9.502
HCG 56b	0.130	0.250	0.750	1.660	10.204
HCG 56c	<0.069	<0.084	<0.500	<0.354	<9.885
HCG 56d	<0.072	<0.087	<0.105	<0.339	<9.480
HCG 56e	<0.078	<0.084	<0.111	<0.342	<9.447
HCG 59a	0.160	0.630	3.700	3.990	10.207
HCG 59b	<0.066	<0.228	<0.135	<0.360	<8.882
HCG 59c	<0.102	<0.156	<0.114	<0.273	<8.879
HCG 59d	0.120	<0.650	<3.670	<3.840	<10.147
HCG 59e	<0.069	<0.198	<0.096	<0.495	<10.482
HCG 61a	<0.072	<0.126	<0.150	<0.333	<8.861
HCG 61b	<0.078	<0.135	<0.129	<0.411	<7.822
HCG 61c	0.290	0.500	5.640	12.010	10.467
HCG 61d	<0.054	<0.090	<0.111	<0.243	<8.772
HCG 62a	<0.090	<0.180	<0.120	<1.910	<9.265
HCG 62b	<0.117	<0.180	0.200	1.720	9.322
HCG 62c	<0.105	<0.162	0.110	<1.320	<9.333
HCG 62d	<0.108	<0.189	<0.090	<0.609	<9.004
HCG 67a	<0.123	<0.261	<0.190	<0.740	<9.811
HCG 67b	0.170	0.280	1.010	2.590	10.333
HCG 67c	0.080	<0.258	<0.210	0.900	<9.752
HCG 67d	<0.102	<0.252	<0.114	<0.387	<9.383
HCG 68a	0.150	<0.114	0.420	1.700	9.019
HCG 68b	<0.123	<0.090	<0.123	<0.312	<8.488
HCG 68c	0.150	0.370	2.340	8.450	9.736
HCG 68d	<0.087	<0.117	<0.156	<0.258	<8.430
HCG 68e	<0.105	<0.060	<0.180	<0.294	<8.488
HCG 69a	<0.096	<0.117	<0.153	<0.267	<9.567
HCG 69b	<0.102	0.440	2.260	4.240	10.734
HCG 69c	<0.102	<0.144	<0.141	<0.300	<9.537
HCG 69d	<0.099	<0.090	<0.144	<0.339	<9.626
HCG 79a	<0.072	0.130	1.280	2.820	9.901
HCG 79b	<0.072	<0.066	<0.130	<0.453	<9.041
HCG 79c	<0.078	<0.069	<0.105	<0.402	<8.912
HCG 79d	<0.063	<0.069	<0.093	<0.399	<8.961
HCG 79e	<0.078	<0.110	<1.080	<2.370	<11.165
HCG 86a	<0.090	<0.162	<0.111	<0.378	<9.2371
HCG 86b	<0.087	<0.114	<0.147	<0.552	<9.351
HCG 86c	<0.069	0.230	0.380	1.670	9.724
HCG 86d	<0.081	<0.123	<0.174	<0.552	<9.409
HCG 87a	<0.120	<0.135	0.200	0.480	9.750
HCG 87b	<0.105	<0.165	<0.170	<0.400	<9.681
HCG 87c	<0.111	<0.156	<0.102	<0.480	<9.624
HCG 87d	<0.118	<0.153	<0.220	<0.460	<9.882
HCG 88a	0.130	0.100	0.470	2.440	9.973
HCG 88b	<0.091	<0.075	0.140	<0.500	<9.3437
HCG 88c	0.080	<0.120	0.360	2.030	9.889
HCG 88d	<0.069	<0.144	0.180	0.770	9.502
HCG 90a	0.440	0.960	5.850	12.420	10.108
HCG 90bd	0.210	0.310	3.430	8.530	9.917
HCG 90c	<0.054	<0.111	<0.144	<0.453	<8.567
HCG 91ad	0.200	0.460	2.220	6.140	10.621
HCG 91b	0.120	0.240	2.060	3.830	10.526
HCG 91c	<0.108	<0.138	<0.800	<1.000	<10.066
HCG 92a	<0.105	<0.210	0.450	<0.750	<7.918
HCG 92b	<0.230	0.220	0.850	2.780	10.069
HCG 92c	0.160	0.230	0.850	2.600	10.191
HCG 92d	0.150	<0.130	<0.850	<0.750	<9.962
HCG 92e	<0.090	<0.162	<0.087	<0.918	<9..547
HCG 96ac	0.660	1.930	5.650	8.440	11.093
HCG 96b	<0.138	0.150	<0.120	<0.573	<9.668
HCG 96d	<0.138	<0.144	<0.141	<0.534	<9.711
HCG 97a	<0.117	<0.195	<0.129	<0.384	<9.416
HCG 97b	<0.105	<0.123	0.150	0.860	9.629
HCG 97c	<0.165	<0.168	<0.123	<0.360	<9.236
HCG 97d	<0.129	<0.195	<0.200	<0.360	<9.383
HCG 97e	<0.117	<0.165	<0.123	<0.426	<9.358
HCG 98a	<0.138	<0.180	<0.123	0.420	<9.509
HCG 98b	<0.138	<0.138	<0.108	<0.400	<9.484
HCG 98c	<0.120	<0.144	<0.114	<0.350	<9.482

TABLE 2—*Continued*

Galaxy	I_{12} (Jy)	I_{25} (Jy)	I_{60} (Jy)	I_{100} (Jy)	L_{FIR} ($L_\odot$)
HCG 98d	<0.129	<0.144	<0.129	<0.460	<10.104
HCG 99a	<0.108	0.100	<0.150	0.430	<9.643
HCG 99b	<0.110	<0.080	<0.183	<0.220	<9.585
HCG 99c	0.100	<0.105	0.110	0.320	9.462
HCG 99d	<0.102	<0.081	<0.123	<0.387	<9.573
HCG 99e	<0.114	<0.108	0.091	0.444	<9.681
HCG 100a	0.120	0.210	2.130	4.020	10.276
HCG 100b	<0.069	<0.117	<0.091	<0.444	<9.122
HCG 100c	<0.072	<0.102	0.300	0.450	9.412
HCG 100d	<0.087	<0.087	<0.123	<0.774	<9.342

[a] The emission in HCG 54 is unresolved. The values correspond to the four galaxies of the group.

class 1, 2, and 3 objects in SS88 and interaction class 2 objects of the *IRAS* Bright Galaxy Sample by Sanders, Scoville, & Soifer (1991). The "strongly perturbed" (SP) galaxy sample consists of 38 galaxies including interaction class 4 objects in SS88, *IRAS* Bright Galaxy Sample interaction class 3 and 4 objects, and closely interacting pairs from Combes et al. (1994). The definitions of "weakly perturbed" and "strongly perturbed" are given in the references listed above—SP galaxies are generally distinguished from WP galaxies as the final stages of mergers. In addition, we have constructed a Virgo Cluster (VC) sample made of 58 bright (Kenney & Young 1988a, 1988b) and faint spirals (Boselli, Casoli, & Lequeux 1995). For three galaxies in the SP sample and 18 galaxies in VC sample, only CO upper limits are available. All the data have been normalized to a common CO-to-H_2 conversion factor (see § 3) and $H_0 = 75$ Mpc^{-1} $km\ s^{-1}$.

Owing to an extensive database available in *IRAS*, the construction of a matching comparison sample for the FIR study is much easier. The FIR comparison sample consists of 212 "class 0" (no companion) galaxies from the Catalog of Isolated Galaxies[4] (CIG) by Karachentseva, Levedeb, & Shcherbanovskij (1973) with redshift and blue luminosity distributions matching that of the HCG sample. The optical luminosity has been derived from the B_T^0 magnitude from the RC3 catalog (de Vaucouleurs et al. 1991), correcting for Galactic absorption (using the extinction value given by Burstein & Heiles 1984 with the reddening law from Savage & Mathis 1979) and internal extinction and *K*-correction (de Vaucouleurs et al. 1991), using the redshift given in NED.[5] The B_T^0 data for HCG galaxies are found in Hickson, Kindl, & Auman (1989b), but they are corrected by 0.1 mag to account for the systematic offset between Hickson et al. (1989b) and RC3 (Moles et al. 1994; Fasano & Bettoni 1994). Data for the other samples are obtained through the NED database.

TABLE 3

PARAMETERS OF COMPARISON SAMPLES[a]

Sample	*N*	log L_B ($L_\odot$)	$\langle\mu_B\rangle$ ($L_\odot$ kpc^{-2})	log M_{H_2} ($M_\odot$)	log L_{FIR} ($L_\odot$)
Isolated.....	68	10.0	7.5	8.9	9.3
WP	43	10.5	7.7	9.6	10.3
SP.....	38	10.7	7.6	10.0	11.0
VC	58	9.9	7.6	8.8	9.3
CIG.....	212	10.2	7.6	...	9.5

[a] L_B has been obtained as explained in § 2.2 and M_{H_2} and L_{FIR} as explained in §§ 3.1 and 3.2, respectively.

The summary of physical properties for all CO and FIR comparison samples is given in Table 3, and the cumulative optical luminosity functions are shown in Figure 2. Given its completeness and depth, the CIG sample is well suited for characterizing the optical luminosity distributions of the

[4] The catalog has been obtained at CDS (Centre de Données Astronomiques de Strasbourg).

[5] The NASA/IPAC extragalactic database (NED) is operated by the Jet Propulsion Laboratory, California Institute of Technology, under contract with the National Aeronautics and Space Administration.

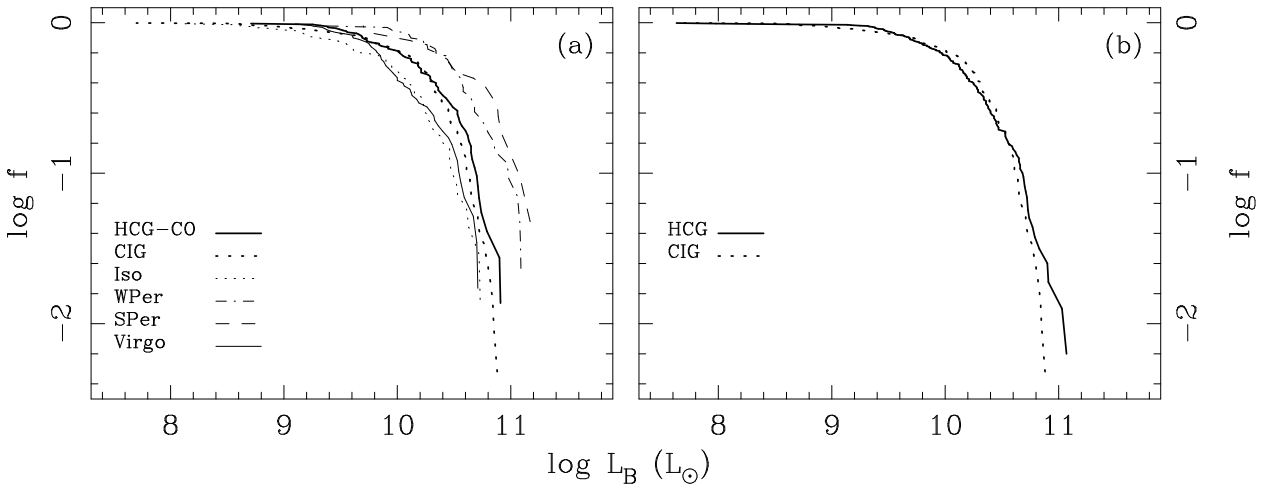

FIG. 2.—(*a*) Cumulative blue luminosity functions for the 80 HCG galaxies observed in CO from our distance-limited sample and the comparison sample galaxies. (*b*) Cumulative blue luminosity functions for the 161 HCG galaxies analyzed with ADDSCAN/SCANPI and 212 galaxies of the CIG comparison sample of isolated galaxies. The HCG and CIG samples have similar luminosity distribution, but the isolated and Virgo cluster samples lack bright galaxies. The WP and SP samples include proportionally more luminous galaxies.

other samples. The optical luminosity distribution of HCG spirals closely coincides with those of the CIG sample (98% probability in a logrank test), and the CO-observed subsample has slightly greater optical luminosity (Fig. 2*a*). Interacting galaxies (WP and SP) show slightly greater optical luminosity because of their biased selection as bright infrared sources (Table 3). Both the isolated CO comparison sample and Virgo Cluster sample lack galaxies at the high-luminosity end. Because $\frac{2}{3}$ of the isolated CO comparison sample come from the distance-limited survey by Sage (1993), this lack of bright spirals is easily explained by the small volume sampled and the local galaxy luminosity function.

While all comparison samples are composed of spiral galaxies only, 39% of our HCG sample (24% for the CO subsample) are E/S0 types. Thus, we analyze spiral and early-type galaxies separately below.

3. CO EMISSION AND MOLECULAR GAS CONTENT AMONG HCG GALAXIES

Molecular hydrogen mass M_{H_2} is derived using a standard CO-to-H_2 conversion, $N_{H_2}/I_{CO} = 3 \times 10^{20}$ cm^{-2} (K km s^{-1})$^{-1}$ and is given by $M_{H_2} = 4.82 I_{CO} d_B^2 M_\odot$, where I_{CO} is velocity-integrated CO flux in K km s^{-1} and d_B is the half-power beam diameter in pc (Sanders et al. 1991). The derived molecular gas masses for the 27 detected and resolved HCG galaxies are listed in Table 1, and they range between 4.6×10^7 $M_\odot$ (HCG 44d) and 2.4×10^{10} $M_\odot$ (HCG 96a, NGC 7674), with a median M_{H_2} of about 2×10^9 $M_\odot$. Three unresolved pairs, HCG 31ac, HCG 38bc, and HCG 90bd, do not have particularly high total gas masses for their optical luminosity.

TABLE 4

RESIDUALS OF M_{H_2} RELATIVE TO THE M_{H_2}-L_B LAW[a]

Sample	Median	Q[b]
ISO	0.04	0.17
WP	0.20	0.21
SP	0.10	0.27
VC	0.20	0.14
HCG-Spiral	−0.32	0.65

[a] See eq. (1) and § 3.1.

[b] Semi-interquartile distance. For a normal distribution $\sigma = \frac{3}{2}$Q.

3.1. *Spiral HCG Galaxies*

In order to search for any enhancement or deficiency in CO emission among the HCG spirals, derived molecular gas mass (M_{H_2}) is plotted against blue luminosity (L_B) for HCG, VC, WP, and SP sample spirals in Figure 3, along with a solid line corresponding to the power-law relation derived from the isolated and field spirals in our earlier study (Perea et al. 1997). Because these two quantities are strongly nonlinearly related, the common practice of normalization by optical luminosity as a measure of molecular gas enhancement (e.g., Braine & Combes 1993) is an inadequate and misleading way to evaluate enhancement or deficiency of molecular gas content, and measuring the deviation from this power-law relation should be a more meaningful test. Accordingly, the median value of the residuals (Δ log M_{H_2}) with respect to the isolated galaxies' template are tabulated in Table 4, along with the semi-interquartile distance that measures the dispersion of the

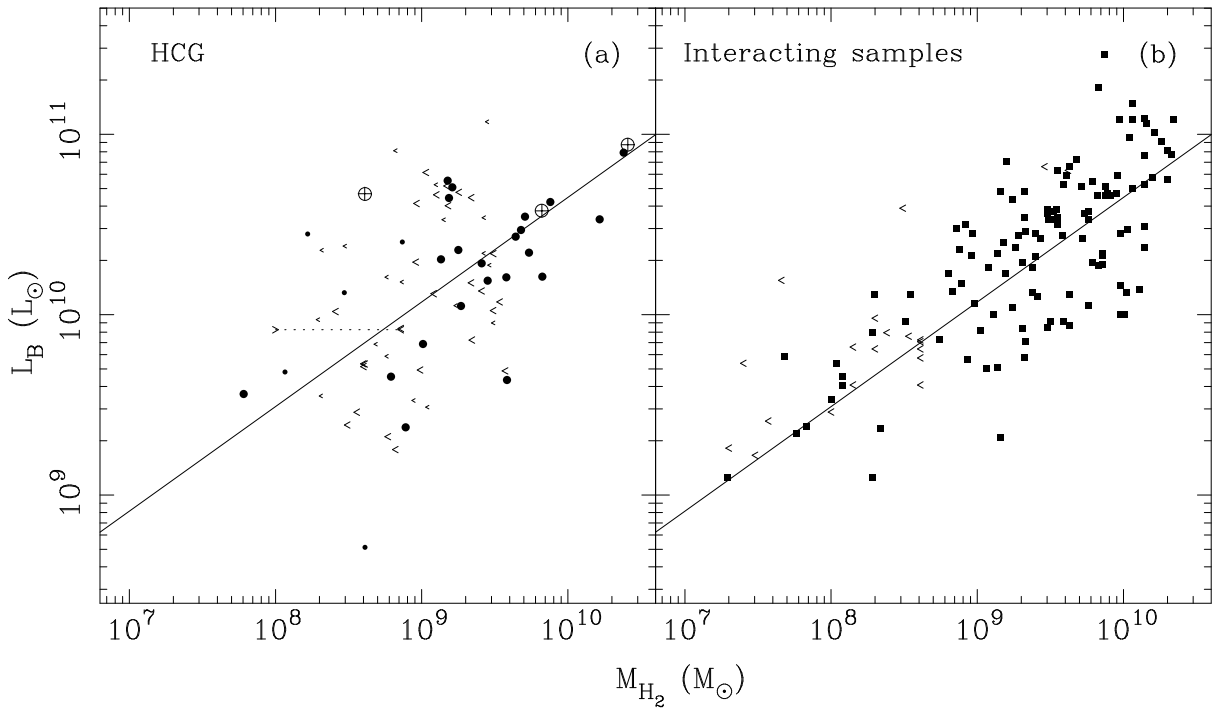

FIG. 3.—Dependence of L_B on M_{H_2} for (*a*) HCG galaxies and (*b*) interacting galaxies belonging to the VC, WP, and SP samples. The solid line corresponds to the best-fit model for the isolated galaxies, log $L_B = (0.57 \pm 0.03)$ log $M_{H_2} + (4.9 \pm 0.6)$ (see Perea et al. 1997). Large symbols in HCG data correspond to late-type galaxies, while small symbols correspond to early-type galaxies. Open triangles are upper limits in H_2. Crossed circles correspond to the summed values for the unresolved pairs H31ac, H38bc, and H90bd. The dotted line marks the range of M_{H_2} of H31b from the single-dish observations (upper limit) and the OVRO data (lower limit; Yun et al. 1997).

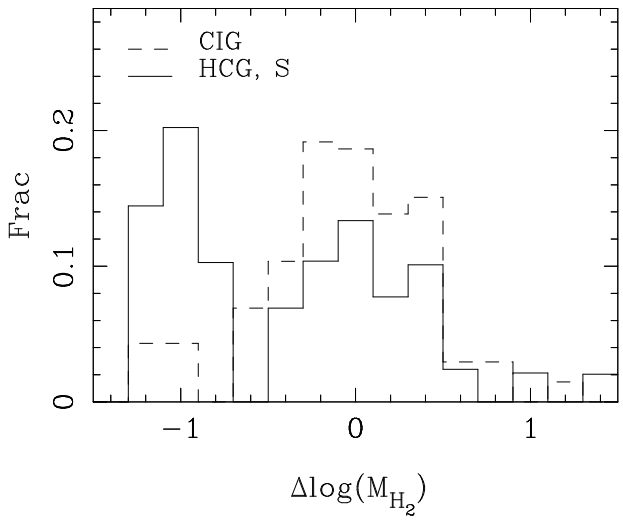

FIG. 4.—Histograms of the residuals $\Delta\log M_{H_2}$ relative to the power-law template of isolated galaxies (*dashed line*) and all HCGs spiral galaxies (*solid line*). The distribution of residuals for the HCG spiral is skewed, and the comparison with the CIG sample suggests that 20% of the HCG spirals are deficient in molecular gas content (by a factor ≥ 10).

distribution [for a normal distribution, $\sigma = (3/2)Q$]. Upper limits have been taken into account using Astronomy Survival Analysis (ASURV).[6] The deviation of the residuals from zero is statistically negligible for both weakly and strongly interacting pairs and cluster galaxies. Figure 3 suggests that HCG galaxies follow the same nonlinear M_{H_2}-L_B relation, but the median value of $\Delta\log M_{H_2}$ is slightly lower (1.3 σ), compared to the CIG sample. The histogram of the residuals of the resolved HCG spiral galaxies (Fig. 4) demonstrates more clearly that there is a subsample of H_2-deficient galaxies, as compared to isolated galaxies. This subsample includes 10 galaxies in total (six upper limits) and accounts for about 20% of all the surveyed HCG spirals.

The observed deficiency of molecular gas among the HCG spirals does *not* result from their being low-metallicity dwarfs—CO-deficient spiral galaxies have $L_B > 10^{10}\ L_\odot$ and a similar luminosity distribution to the WP and SP sample. A telling clue to the physical reality and possible causes of the CO deficiency is that all three observed galaxies in HCG 92 (b, c, and d) are CO deficient—with nearly 10 times less CO emission than is expected for their luminosity. Similarly, the unresolved pair H31ac, which is also one of the densest groups in the Hickson catalog, displays a factor of 30 deficiency in CO emission for its optical luminosity. We have studied both HCG 31 and HCG 92 with the OVRO interferometer (Yun et al. 1997) in order to understand better their faint CO emission, and we found that the CO emission is highly asymmetric and disturbed. Strong tidal disruptions likely play an important role in producing such morphology, but the actual physical mechanism for producing reduced CO emission is uncertain. Possible explanations for the CO deficiency in these most compact (thus presumably the most evolved) groups include the exhaustion of the gas supply through tidally induced massive star formation; they are discussed further in § 6.

[6] The Astronomy Survival Analysis (ASURV) Rev 1.2 package is a generalized statistical analysis package that implements the methods presented by Feigelson & Nelson (1985) and Isobe, Feigelson, & Nelson (1986) that are described in detail in Isobe & Feigelson (1990) and LaValley, Isobe, & Feigelson (1992).

3.2. *E/S0 HCG Galaxies*

Among the distance-limited complete sample of HCG galaxies for which CO emission is examined, there are 24 early-type galaxies with Hubble type E or S0, and five galaxies are detected with inferred molecular gas masses of 1.2–24.8 $\times 10^8\ M_\odot$. Because only a limited number of ellipticals have been observed in CO previously, the statistical importance of a 20% detection is not clear. However, such a presence of cold gas in elliptical galaxies is generally attributed to the merger or accretion of a gas-rich companion (Wiklind, Combes, & Henkel 1995; Huchtmeier & Tammann 1992; Lees et al. 1991). The two CO-detected elliptical galaxies HCG 90b and HCG 90c are very close to an irregular galaxy HCG 90d, which is in projected contact with HCG 90b and joined by a tail-like feature with HCG 90c (Longo et al. 1994). HCG 90b and HCG 90d are unresolved by our beam, and the spectrum (Fig. 1) is well centered at the velocity of the irregular galaxy. However, the CO observations of HCG 90b by Huchtmeier & Tammann (1992) with a smaller beam also support the fact that a significant part of the molecular gas is associated with the elliptical galaxy, since their beam does not include HCG 90d. This may also be the case in HCG 90c, as suggested by its optical bridge with HCG 90d. This observation is consistent with a general expectation that mergers or accretions can readily occur in a compact-group environment. Another CO-detected source, HCG 68a, is a lenticular galaxy that is also an X-ray and FIR source. It is also in close contact with an elliptical companion, HCG 68b, and the only spiral companion in the group is 4′ away. HCG 61a was originally classified as a spiral by Hickson (1993), but it is classified as an elliptical by Rubin, Hunter, & Ford (1991) and as a lenticular in RC3. The molecular gas in this galaxy probably originated from a late-type companion, such as HCG 61c (Sbc).

4. INFRARED PROPERTIES OF HCG GALAXIES

4.1. *Far-Infrared Luminosity Distribution*

The UV and optical photons emitted by massive young OB stars are absorbed and reradiated in the far-infrared by dust. Therefore, infrared emission provides a vital clue in the study of star formation activity and the surrounding medium. FIR luminosity is computed from the *IRAS* measurements as $\log L_{FIR}/L_\odot = \log \mathrm{FIR} + 2 \log D + 19.495$, where D is distance in Mpc and $\mathrm{FIR} = 1.26 \times 10^{-14}(2.58 I_{60} + I_{100})$ W m^{-2} (Helou et al. 1988). The λ 12, 25, 60 and 100 μm fluxes and derived FIR luminosity (L_{FIR}) are listed in Table 2. A total of 161 HCG galaxies are examined, and five pairs (HCG 31ac, HCG 38bc, HCG 90bd, HCG 91ad, and HCG 96ac) and one quartet (HCG 54) are still unresolved by ADDSCAN/SCANPI. For these cases, the sums of FIR fluxes are listed in Table 2. The number of *IRAS*-detected individual galaxies and unresolved pairs/quartet are respectively 35/5 at 12 μm ($\geq$25%), 36/6 at 25 μm ($\geq$26%), 61/6 at 60 μm ($\geq$42%), and 55/6 at 100 μm ($\geq$38%). Among the 75 galaxies undetected by *IRAS*, 67 galaxies (75%) are classified as E or S0 and are not expected to emit in FIR above the *IRAS* sensitivity. The remainder have $m_B > 14.7$, which is below the *IRAS* detection limit derived through the L_{FIR}-L_B relationship (see Fig. 5).

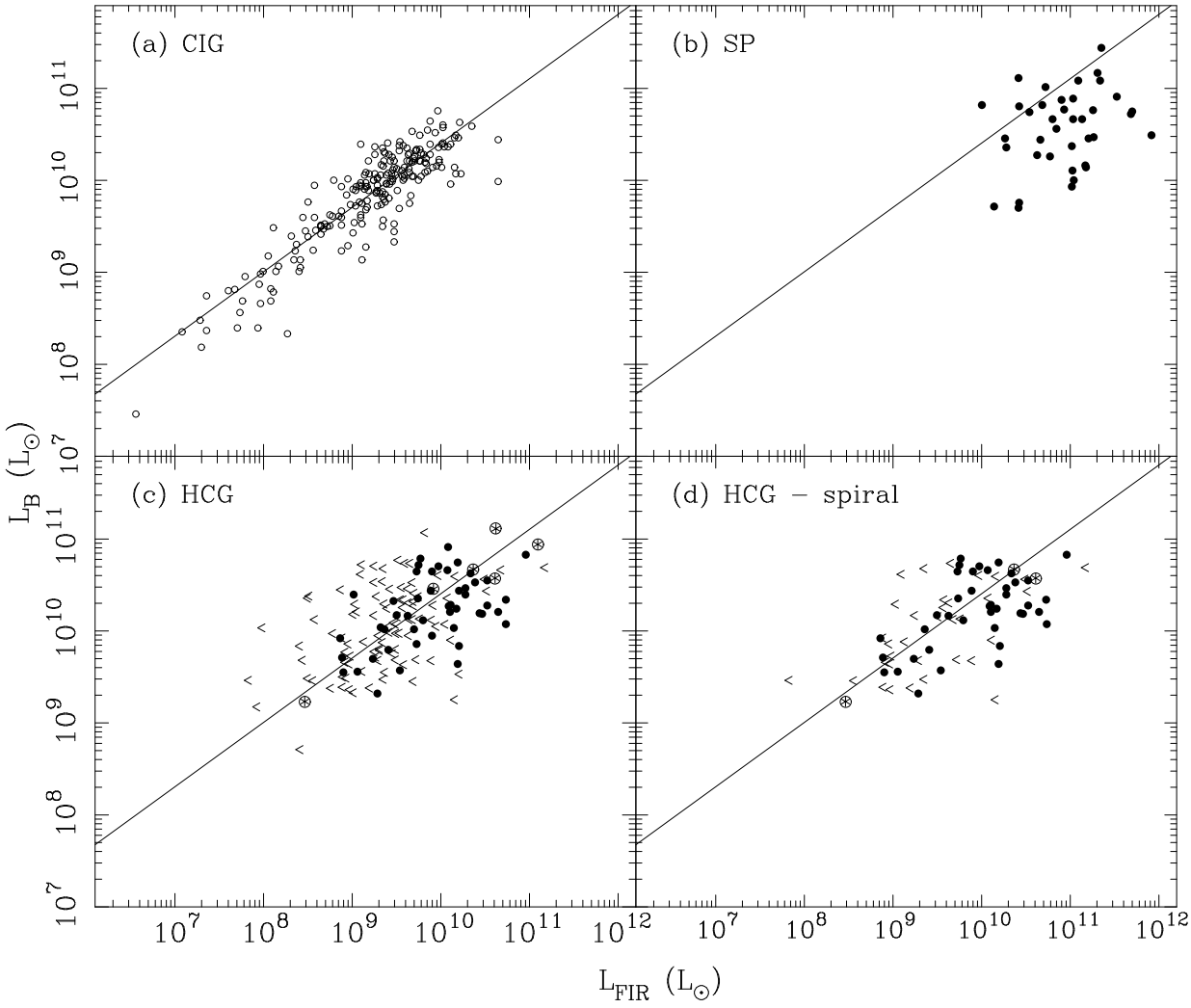

FIG. 5.—Dependence of L_B on L_{FIR} for (*a*) CIG sample, (*b*) SP sample, (*c*) all HCG galaxies, and (*d*) HCG spirals only. The solid line corresponds to the power law best describing the CIG sample. Open triangles are upper limits in FIR. Encircled points are the unresolved pairs with summed values. In comparison, only the SP sample shows significant FIR excess from the template relation derived from the isolated galaxy sample.

In the conservative assumption that FIR emission in unresolved pairs comes from only one galaxy, 68% (25/37) of the groups contain more than one *IRAS* source, and 29% (10/37) contain at least three *IRAS* sources. This confirms the inference made by Sulentic et al. based on source statistics that more than one galaxy contributes to the FIR emission detected by *IRAS*. HCG 46 is the only HCG without any FIR source detected by SCANPI ($\sigma \sim 30$ mJy at 60 μm). For the statistical analysis of FIR properties, 149 galaxies in 37 Hickson groups are included, after excluding 12 galaxies with a discordant redshift.

The FIR luminosity of HCG galaxies has been evaluated in a similar way as the molecular content. There is a known close correlation between L_{FIR} and L_B (see Bothun, Lonsdale, & Rice 1989; Dultzin-Hacyan, Masegosa, & Moles 1990), and the blue luminosity of the CIG sample of isolated galaxies can be described as

$$\log L_B = (0.70 \pm 0.03) \log L_{FIR} + (3.4 \pm 0.2) . \quad (1)$$

This agrees well with the relation found for the isolated galaxy sample of Perea et al. (1997), $L_B \propto L_{FIR}^{0.65 \pm 0.09}$. Again, the normalization using optical luminosity still leaves a residual dependence of L_{FIR}/L_B on L_B, so that brighter galaxies will have intrinsically larger values for this ratio independently of environmental effects. The presence of any FIR enhancement among HCG galaxies is examined by comparing their L_B-L_{FIR} distribution to the CIG and SP comparison sample in Figure 5. The well-known FIR enhancement among the SP sample is clearly shown in Figure 5*b*. The data for all HCG galaxies are shown in Figure 5*c*, and HCG spiral galaxies are shown separately in Figure 5*d*. These figures suggest that HCG spiral galaxies follow the same trend as the CIG galaxies. The distribution of residuals $\Delta \log L_{FIR}$ relative to the power law in equation (1) is shown in Figure 6*a* for the CIG and HCG spirals samples, and the corresponding median and semi-interquartile distances are listed in Table 5. Both samples have the same median value, with a larger dispersion for the HCG galaxies. We conclude that HCG spirals as a group do not show a significant enhancement in their FIR emission with respect to CIG galaxies. If only the detected galaxies are included in the analysis, an apparent enhancement by a factor of 3 is suggested (see Table 5; Fig. 6*b*). However, this is due to a well-known luminosity and detection bias, and all upper

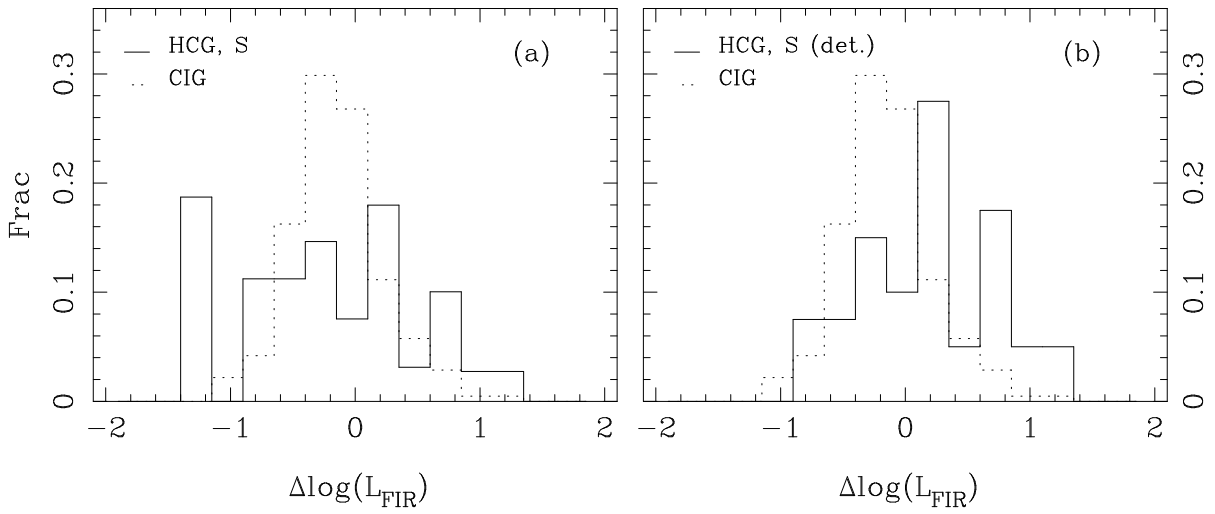

FIG. 6.—Histograms of the residuals $\Delta\log L_{\rm FIR}$ relative to the power law derived from the CIG sample (*dashed line*). The solid lines correspond to (*a*) all HCGs spiral galaxies and (*b*) only HCGs spirals detected at both 60 μm and 100 μm bands. The broader distribution of residuals for the HCG spirals is in part due to larger associated measurement uncertainties, but it may also reflect real physical effect. When only the detected objects are considered (*b*), an impression of an apparent FIR enhancement may be deduced, and all upper limits should be included in this analysis.

limits for the low–FIR luminosity galaxies have to be taken into account for a proper analysis.

In summary, no significant enhancement in FIR emission is found among the HCG spirals. This contradicts the earlier findings by Hickson et al. (1989b), and the reason for the contradiction results in part from the presence of more than one FIR source in many of the groups, as suggested by Sulentic & de Mello Rabaça (1993) and Venugopal (1995). At least 68% of the groups contain more than one *IRAS* source, 29% have at least three *IRAS* sources, and assigning FIR fluxes to a single galaxy have led Hickson et al. (1989b) to overestimate the FIR emission per galaxy.

Only 17 out of 71 early-type galaxies are detected by *IRAS*, and this is similar to the detection rate found for other early-type samples (Marston 1988). FIR emission from early-type galaxies is usually attributed to dusty ellipticals and S0s as a result of merger or accretion processes (Marston 1988). Six galaxies are detected at least in three *IRAS* bands, and they all show peculiarities. Four of these galaxies are the first ranked in the group or the brightest early-type member. HCG 37a is a radio and X-ray source with a rapidly rotating disk in the center, and [N II] emission and ellipticity variations are reported (Rubin et al. 1991; Bettoni & Fassano 1993). The S0 galaxy HCG 56b has a warped disk connected with that of the S0 companion HCG 56c and is also a radio continuum source (Rubin et al. 1991; Menon & Hickson 1985). HCG 68a is a radio and X-ray source and has associated 21 cm H I emission (Williams & Rood 1987), and CO emission is detected by our survey. HCG 79a is a radio continuum and 21 cm H I source and is crossed by a strong dust lane, suggesting an accretion from its spiral companion HCG 79d. HCG 86c is classified as SB0 and is detected in 25 μm, but spectroscopic measurements of the Mg_2 band suggest a metallicity that is characteristic of a normal elliptical galaxy ($M_g = 0.29$, $\sigma_v = 173$ km s^{-1}).

TABLE 5

RESIDUALS OF $L_{\rm FIR}$ RELATIVE TO THE $L_{\rm FIR}$-L_B LAW[a]

Sample	Median	Q
CIG.....	−0.17	0.20
HCG, S.....	−0.22	0.50
HCG, S (det)[b].....	0.22	0.43

[a] See eq. (1) and § 4.1.
[b] Galaxies detected in FIR.

4.2. I_{25}/I_{100} Ratio: An Indicator of Enhanced Nuclear or Starburst Activity

The flux ratio between *IRAS* 25 and 100 μm bands, I_{25}/I_{100}, is a useful indicator of nuclear or starburst activity (Dultzin-Hacyan et al. 1988, 1990). The histograms of the I_{25}/I_{100} ratio for the CIG sample and HCG spirals are shown in Figure 7, excluding the unresolved pairs. The data for a sample of H II, blue compact, clumpy irregulars, and starburst galaxies from Dultzin-Hacyan et al. (1990) are also shown for comparison. Only the galaxies detected at least at 100 μm are considered, since the ratio becomes too uncertain if undetected at 100 μm. Among the samples considered, 45% of the CIG sample galaxies and 72% of the HCG galaxies are detected at the 25 μm band. Galaxies with only upper limits at 25 μm are also included in the analysis.

The distributions of the I_{25}/I_{100} ratio for the CIG and HCG samples are different at the 99.99% level, according to the logrank and Peto-Prentice generalized Wilcoxon tests included in ASURV, which are known to be the most robust in measuring the degree of discrepancy between two cumulative distribution functions in the presence of lower or upper limits. The median value of the I_{25}/I_{100} ratio for HCG galaxies is a factor of 2 larger than for the CIG sample (Table 6) and similar to the compact starburst sample from Dultzin-Hacyan et al. (1990). Including only the 100 μm–detected galaxies in the analysis has little effect

TABLE 6

PARAMETERS OF $\log I_{25}/I_{100}$

Sample	Median	Q
CIG.....	−1.38	0.12
HCG, S.....	−1.12	0.17
SB + H II.....	−1.00	0.18

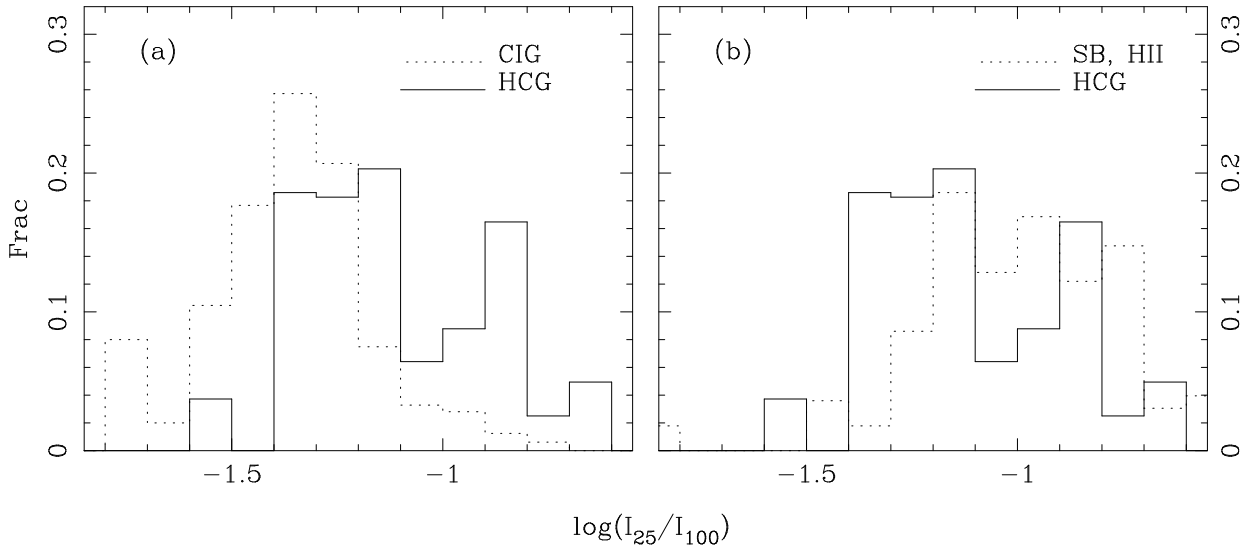

FIG. 7.—Histogram of log I_{25}/I_{100} for (*a*) CIG sample (*dotted line*) and HCG galaxies (*solid line*), and (*b*) starburst and H II galaxies from Dultzin-Hacyan et al. (1990; *dashed line*).

on this conclusion, because the comparisons of the cumulative functions including all data show that the enhancement in the HCG sample is in the 25 μm emission, while the 100 μm cumulative luminosity functions are identical (see Fig. 8).

The enhanced I_{25}/I_{100} ratio among HCG galaxies indicates an enhanced and localized UV radiation field, due either to intense local star formation or to the presence of an active galactic nucleus (AGN). The number of known Seyfert galaxies among HCG galaxies is small (9% in our complete sample), and therefore the bulk of the excess seems to be caused by local starbursts, presumably in the nuclear region, as suggested by the enhanced nuclear radio continuum emission (Menon 1995). A detailed spectrophotometric study is needed to confirm this result. This evidence for enhanced localized starburst is still compatible with the conclusion of a normal level of FIR emission among HCG galaxies, if the activity responsible for enhanced 25 μm emission is localized compared to the overall distribution of gas and dust in each galaxy, as in H II and Markarian galaxies.

5. STAR FORMATION EFFICIENCY ($L_{\rm FIR}/M_{\rm H_2}$)

A linear correlation between the observed FIR luminosity and the total CO luminosity is well documented by various previous surveys, and the $L_{\rm FIR}/M_{\rm H_2}$ ratio is sometimes referred to as "star formation efficiency" (SFE; see Young & Scoville 1991 and references therein). The total FIR luminosity of the CO-observed subsample is plotted as a function of total derived H_2 mass, along with those of the comparison galaxies in Figure 9, and the results are quantified through the statistical analysis described in Perea et al. (1997) in order to examine whether HCGs have a star formation efficiency that is similar to that of strongly interacting galaxies. The "correlation" between CO and FIR is a rather broad tendency, spanning *2 orders of magnitude* in the $L_{\rm FIR}/M_{\rm H_2}$ ratio. On the other hand, individual interaction subclasses, with the exception of the SP sample,

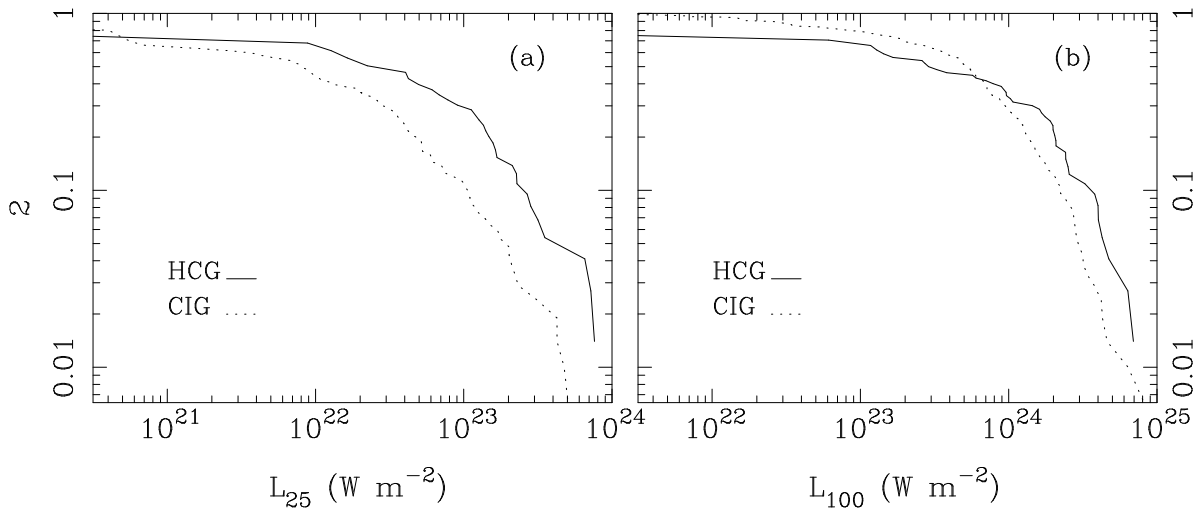

FIG. 8.—Cumulative luminosity distributions for the HCG spiral and CIG samples at (*a*) 25 μm and (*b*) 100 μm. While the 100 μm distribution is similar for the two samples, there is a clear enhancement in 25 μm emission among the HCG sample.

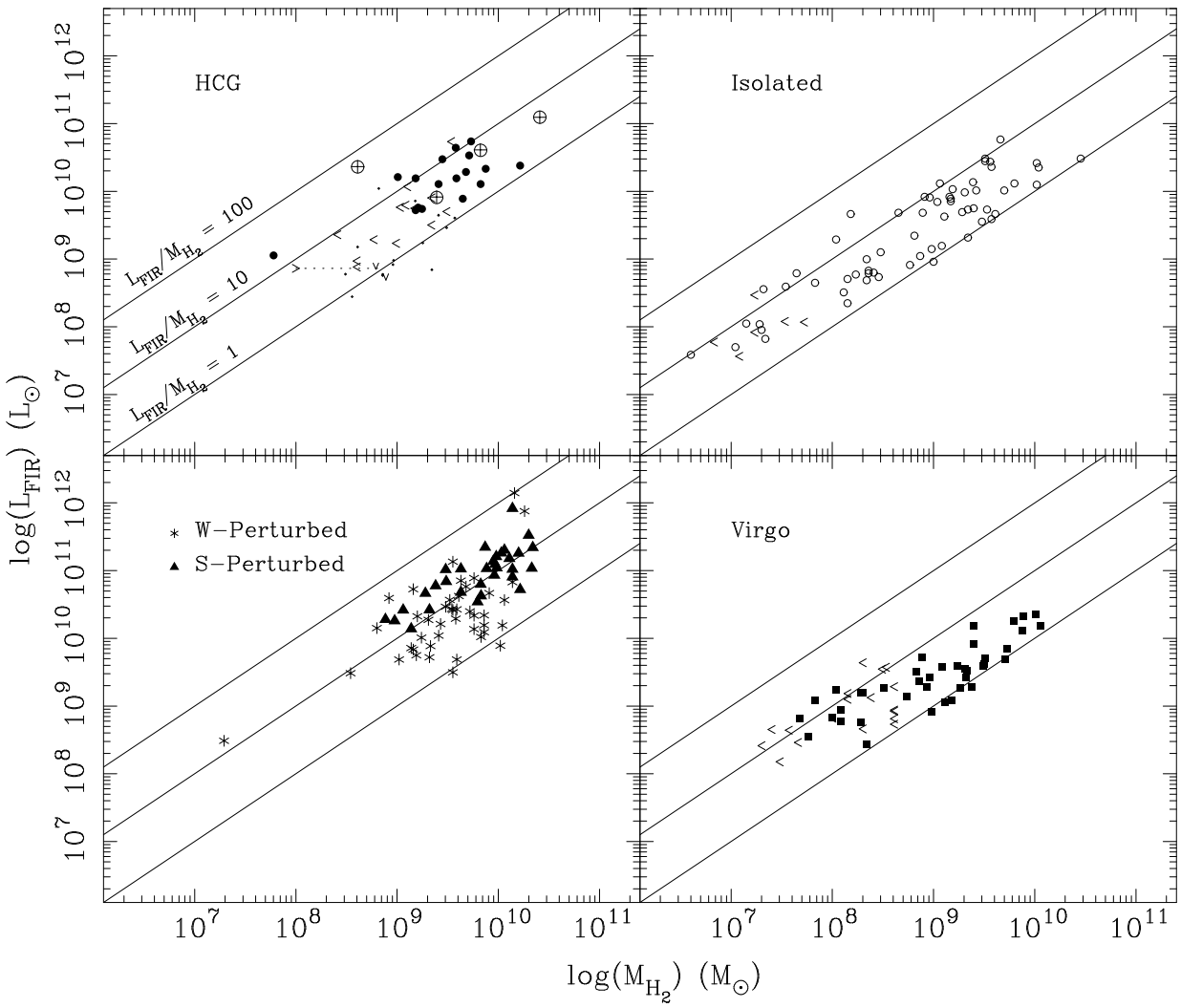

FIG. 9.—Dependence of L_{FIR} on M_{H_2} for HCG galaxies and three interacting comparison samples. The plotted lines correspond to the ratios L_{FIR}/M_{H_2} = 1, 10, and 100 $L_\odot\ M_\odot^{-1}$, a measure of efficiency in converting gas to luminosity (e.g., Sanders et al. 1991). The dots in the HCG plot are upper limits on both axes, and open triangles are upper limits. The dotted line corresponds to the range of M_{H_2} for H31b from the single-dish observations (upper limit) and the OVRO data (lower limit; Yun et al. 1997).

occupy a much narrower strip of area between L_{FIR}/M_{H_2} = 1 and 10 $L_\odot/M_\odot$ in each plot. The WP sample galaxies, which show a marginal excess in SFE (Perea et al. 1997), also lie mainly in the same region. Therefore they all seem to share a common efficiency in converting gas into FIR luminosity. The only exception is the SP subsample, which displays an enhanced SFE, as already known (L_{FIR}/M_{H_2} = 5–40 $L_\odot/M_\odot$; Sanders et al. 1986; SS88; Young & Scoville 1991). Since molecular gas content is independent of interaction environment, this increase in SFE is really a result of greater FIR emission. The HCG galaxies with a normal level of molecular gas content and FIR emission thus show no measurable enhancement in SFE. One exception is HCG 31ac, which shows a significantly high L_{FIR}/M_{H_2} ratio of 57 $L_\odot/M_\odot$, characteristic of a strongly interacting or merging starburst galaxy. This may be caused by low CO luminosity (see below), but this pair is also undergoing a strong tidal interaction and a burst of star formation.

6. DISCUSSION

6.1. *Tidal Interactions and Induced Activities in the Compact-Group Environment*

Hickson compact groups represent a unique environment with high galaxy density and low velocity dispersion that is comparable to the cores of rich clusters such as Coma. In contrast to the cluster environment, the majority of our HCG sample consist largely of late-type galaxies with a Hubble type composition that is similar to the field and loose groups, and they represent the highest density environment for late-type galaxies. The main objective of this paper is to address whether frequent tidal encounters that may occur in these groups induce activities and transformations of the member galaxies.

Enhancement of CO emission and thus molecular gas content for interacting galaxies has been suggested previously in the literature, perhaps by inflow of cold gas from

reservoirs outside or within (e.g., Braine & Combes 1993; Combes et al. 1994), and similar enhanced CO emission may be expected if tidal interactions are frequent among HCG galaxies. However, CO emission among the HCG spiral galaxies follows largely the same nonlinear behavior derived from the samples of isolated spiral galaxies, and there is no evidence for any enhanced molecular gas content among HCG galaxies (see Fig. 3). Previous reports of enhanced CO emission among interacting galaxies are likely due to the strongly nonlinear L_B-M_{H_2} relationship and sample selection that is biased toward high-luminosity galaxies (Perea et al. 1997). Surprisingly, 20% of HCG spiral galaxies show a *deficiency* of CO emission: we discuss below possible causes for the reduced CO emission and molecular gas content.

Enhanced star formation and an associated high FIR luminosity in gas-rich spiral galaxies undergoing a tidal interaction have been well documented by both observational and numerical studies (e.g., Larson & Tinsley 1978; Bushouse 1987; SS88; Sanders et al. 1991; Surace et al. 1993; Mihos & Hernquist 1996). In the dense spiral-rich environment constituted by HCGs, we expect a priori an enhanced level of FIR emission if tidal encounters are frequent. On the contrary, the level of FIR emission is comparable to that of isolated galaxies, Virgo spirals, and weakly interacting pairs, and only strongly perturbed pairs and mergers show clear signs of enhanced FIR emission (see § 4.1; Perea et al. 1997). An explanation may lie in the fact that only 10% of our distance-limited complete sample of HCG galaxies show clear signs of strong tidal disruption such as tails and bridges; their similar level of FIR emission to isolated and weakly interacting samples must then result from the fact that most tidal disruptions in a compact-group environment are mild in nature.

This weak dependence of induced star formation on environment is likely due to the highly nonlinear nature of tidal disruption. In the impulse approximation of tidal disruption, the tidal acceleration experienced scales as $1/vr^2$, where v is the encounter velocity and r is the impact distance. In a cluster the encounter velocities are much larger ($v > 1000$ km s^{-1}), and the resulting tidal disruption and tidally induced activities would be 5–10 times smaller than for an interacting pair with the same impact distance. Little or no enhancement in FIR emission among Virgo Cluster spirals is consistent with this expectation. In the compact-group environment, velocity dispersions are low, comparable to the orbital speed of interacting pairs, while the galaxy density may be as high as in the cores of rich clusters (Hickson et al. 1992). Therefore, one may expect a level of tidally induced activity that is similar to or even higher than in interacting pairs. The level of FIR emission among the HCG galaxies is similar to that of the isolated sample, and one may conclude that small–impact distance collisions are rare in a compact-group environment, and that even a high frequency of encounters in a compact group may have relatively little impact on the overall level of induced activity.

Sulentic & Rabaça (1994) have proposed H I deficiency (Williams & van Gorkom 1995; Huchtmeier 1997) and thus a low fuel supply for star formation as the explanation of a level of star formation among HCG galaxies that is similar to that of the isolated sample. The H I deficiency is not likely a direct explanation, since stars form in molecular gas whose abundance is found to be mostly normal (§ 3.1). Jog & Solomon (1992) suggest that during direct encounters, atomic clouds collide and produce an overpressure in hot ionized gas and trigger a burst of star formation, produced by a radiative-shock compression of the outer layers of GMCs. For the HCG galaxies that are H I deficient, this induced star formation process may be quenched.

A factor of 2 enhancement in the I_{25}/I_{100} ratio is detected among the HCG galaxies, and we have interpreted this as H II galaxy–like localized starburst, probably in the nuclear region, based on the radio continuum observations by Menon (1995). The enhancement in 25 μm emission among the HCG galaxies may be the result of frequent (but weak) tidal encounters in the compact-group environment.

6.2. *CO Deficiency in HCG Spirals*

While the majority of the HCG spiral galaxies show levels of molecular gas content similar to those of isolated spirals, some 20% of the HCG spirals show deficiency of CO emission and presumably low molecular gas content. While the total number of CO-deficient galaxies is small, telling evidence for their special nature is that these CO-deficient spirals seem to occur in specific groups (e.g., HCG 31, HCG 92) and not randomly. This deficiency may be related to the dynamical evolution of the individual groups, since the prominent CO-deficient groups are also the most dynamically evolved groups—as evidenced by the common H I envelope in HCG 31 (Williams, McMahon, & van Gorkom 1991) and extended H I, stellar, and X-ray emission in HCG 92 (Shostak, Allen, & Sullivan 1984; Sulentic, Pietsch, & Arp 1995). High-resolution mapping of CO emission in two CO-deficient groups, HCG 31 and HCG 92, using the OVRO millimeter interferometer have revealed highly disturbed molecular gas distribution in the individual galaxies (Yun et al. 1997).

Similar deficiency of H I emission among HCGs is also reported by Williams & Rood (1987) and by Huchtmeier (1997). For the H I deficiency, tidal stripping of H I disks by frequent interactions in the group environment offers a plausible explanation, but tidal stripping of molecular gas is less likely, since molecular gas is usually concentrated in the inner disks. This has been suggested as being the case for the spirals in the Virgo Cluster, where the H I gas has been found to be stripped from the outer disk regions (Stark et al. 1986), while the molecular gas content is not changed (Young et al. 1989; Perea et al. 1997). Gas exhaustion through star formation is a possible mechanism that may be responsible for the CO deficiency among the most strongly interacting groups. In simulations of the gas hydrodynamics of gas-rich mergers, Mihos & Hernquist (1996) note the difficulty of achieving very high gas density in strongly interacting systems because of fast and efficient exhaustion of the gas supply by star formation. In normal disk galaxies the resupplying of the ISM is achieved through the recycled material from evolved stars and the accretion of cold gas from the outer disks and halo. Among the galaxies frequently perturbed by other companions, this resupplying of cold gas may be disrupted if the outer H I disks are stripped. If the observed CO deficiency is related to the dynamical evolution of compact groups while the gas-rich, spiral-dominated groups represent a dynamically younger stage still in the process of collapsing, then their ratio may indicate the relative timescales for the initial infall phase to the final rapid–group evolution phase. Because of possible selection biases in the group identification, as well as poor statistics on the CO deficiency, this ratio is not well con-

strained, but one may estimate from the observed ratio (a lower limit) that the rapid-evolution phase may be at least $\frac{1}{4}$ as long as the phase during which a group is recognized as a spiral-rich "compact group."

Low metallicity is not likely an important reason for the low CO luminosity observed among HCG spirals, since the CO deficiency is detected among relatively bright spirals in our HCG sample ($L_B > 10^{10}\ L_\odot$). Optically thick in nature, CO emission is a robust tracer of moderate metallicity variations as well as moderate increases in the UV radiation field associated with intense star formation activity (see Wolfire, Hollenbach, & Tielens 1993 and references therein). CO molecules may suffer significant photodissociation in low–gas column density regions, such as in the starburst region in HCG 31.

6.3. *Early-Type Galaxies*

The nature of CO and FIR emission in early-type galaxies in HCGs is difficult to analyze, since little comparison data exists in the literature. The majority of existing CO and FIR studies of early-type galaxies are mostly for unusual galaxies with bright FIR emission. There is strong evidence that the CO- and FIR-detected early-type galaxies in HCGs are also unusual and perhaps closely tied to their compact-group environment. For example, all of the CO-detected HCG elliptical galaxies in the X-ray–observed groups also show associated diffuse X-ray emission, suggesting perhaps that they belong to the more evolved groups. Evidence for tidal capture from a gas-rich companion or the accretion of a gas-rich dwarf also exists in some cases, such as for HCG 90 (see § 3.2). Whether the observed frequency is any higher than the field or loose group environment is uncertain, but the presence of a number of early-type galaxies with unusual CO and FIR properties lends further support to the frequency of tidal interactions in a compact-group environment.

7. SUMMARY

We have conducted a study of a distance-limited complete sample of Hickson compact group galaxies for CO and FIR emission in 80 and 161 galaxies, respectively, and found that the CO and FIR emission in HCG galaxies are at a level that is similar to the comparison samples of isolated, Virgo Cluster, and weakly interacting galaxies. About 20% of HCG spiral galaxies are deficient in CO emission, and gas exhaustion through star formation along with gas reservoir reduction through tidal stripping of the outer H I disks may offer an explanation. While the FIR emission from HCG spirals as a group is indistinguishable from the comparison samples of field and Virgo Cluster spirals, some evidence for localized intense bursts of star formation, probably in the circumnuclear regions, is found in the enhancement of the I_{25}/I_{100} ratios. Some groups, such as HCG 31 or HCG 92, may be well advanced in their evolution if their CO deficiency is dynamical in nature. Along with the CO and H I deficiency in some of the HCGs, the presence of early-type galaxies with significant CO and FIR emission lends a further support to frequent tidal interaction and accretion events in the compact-group environment.

The authors thank the staff of the NRAO 12 m telescope and the Haystack observatory for their assistance with the observations. We also thank D. Benford and J. Girart with the CO observations at the CSO and Haystack observatory. L. V. M. acknowledges financial support and hospitality from the Harvard-Smithsonian Center for Astrophysics. J. P., A. O., and L. V.-M. are partially supported by DGICYT (Spain) grants PB93-0159 and PB96-0921 and Junta de Andalucía (Spain). M. S. Y. is supported by the NRAO Jansky Research Fellowship.

APPENDIX A

SCANPI STATISTICS ON RADIO-LOUD QSOs

The positional accuracy and possible source confusion, as well as the calibration of the *IRAS* SCANPI data, are tested by analyzing the data on radio-loud QSOs. A list of candidate QSOs with *IRAS* detection was compiled from the literature (Neugebauer et al. 1986) and from our own search (in collaboration with L. Armus). This list is further reduced to 29 objects by requiring that they be radio-loud objects and VLA calibrators—this extra step ensures having highly accurate coordinate information on each source. SCANPI data are obtained and analyzed in the same manner as for the HCG sample (see § 2.3), and 27 out of the 29 objects in the list are detected with a S/N of 3 or better at 60 μm (Table 7). Both for this analysis and in the source identification for the HCG sample, the 60 μm band is used because of its superior sensitivity over the other bands, both in raw sensitivity and favorable spectral energy distribution among these extragalactic sources.

The calibration of the SCANPI data is checked by comparing the measured flux to the pointed observations by Neugebauer et al. (1986) and is shown in Figure 10. In general, published and new SCANPI fluxes agree well, with a few exceptions. There are four objects (out of 19 plotted) that show significant disagreement. While measurement inconsistencies are possible, a likely explanation is that many of these sources are known BL Lac or optical variables whose observed flux may fluctuate by a factor of a few on a timescale of several months, and the observed disagreement is well within this intrinsic variability. Therefore, the calibration of SCANPI data appears reliable.

The "miss" parameter given by the SCANPI processor is the offset in the source position along the average scan direction with respect to the specified source position, and this parameter is used as the primary measure of source identification. A histogram of the miss parameter for the 27 detected QSOs of the sample is shown in Figure 11. While the majority of the points lie clustered around the zero offset, two objects are detected with a miss parameter greater than 20″. A source confusion is suspected for these two, and Digitized Sky Survey plates are examined for all detected sources. As summarized in Table 7, potential source confusion exists for several objects, and the two highly discrepant objects appear indeed to result from source confusion and/or low S/N in the measurements. Excluding these two objects, the standard deviation of the "miss" parameter for the remaining 25 objects is 6.″7—about 1/10 of the intrinsic spatial resolution, which is reasonably expected. The

TABLE 7

SCANPI SUMMARY OF RADIO[a] QSOs

Source	$I_{60\,\mu}$(N86) (mJy)[b]	$I_{60\,\mu}$(SCANPI) (mJy)	S/N	Miss (arcsec)	Note
0007+106.....	213 ± 8	320 ± 56	5.7	−0.6	
0109+224.....	...	180 ± 39	4.4	−9.0	
0134+329.....	770 ± 9	830 ± 34	24.1	+0.0	
0234+285.....	187 ± 18	190 ± 56	5.7	−14.4	
0420−014.....	271 ± 16	450 ± 50	3.9	−2.4	
0438−436.....	120 ± 14	150 ± 33	4.6	+27.6	Four bright objects within 1′.5
0454−234.....	...	160 ± 30	5.2	−8.4	
0537−441.....	631 ± 25	460 ± 27	16.8	−2.4	
0736+017.....	133 ± 8	0 ± 52	0.0	...	
0738+313.....	145 ± 8	210 ± 34	6.1	+1.8	
0742+318.....	112 ± 8	100 ± 42	2.2	−27.6	Three or four similarly bright objects within 30″
0748+126.....	205 ± 17	250 ± 25	9.7	−28.8	Several brighter objects within 1′
1219+285.....	...	250 ± 48	5.1	−8.4	A faint companion galaxy
1226+023.....	1805 ± 14	2060 ± 43	47.4	−1.8	
1253−055.....	...	220 ± 40	5.4	+6.0	
1404+286.....	652 ± 21	740 ± 35	20.6	−1.8	
1448+634.....	260 ± 40	270 ± 45	6.0	−1.2	
1514−241.....	...	360 ± 35	10.0	−11.4	Spatially extended (>1′)
1641+399.....	766 ± 18	720 ± 30	23.8	−1.2	
1652+398.....	...	90 ± 20	4.5	−3.6	
1656+053.....	...	220 ± 26	8.2	−2.4	
1739+522.....	...	100 ± 22	4.5	+6.6	
2059+034.....	174 ± 12	120 ± 40	3.0	+9.6	Several faint sources within 1′
2201+315.....	126 ± 9	160 ± 46	3.4	+12.0	
2223−052.....	951 ± 16	680 ± 45	14.8	+1.8	
2251+158.....	179 ± 19	200 ± 59	3.4	+9.0	A bright companion
2254+074.....	155 ± 20	230 ± 38	6.1	−2.4	
2314+038.....	672 ± 52	720 ± 39	16.3	+8.4	A bright galaxy at 45″ north
2334+282.....	...	190 ± 26	7.2	−0.6	

[a] The coordinates for the radio QSOs are taken from the VLA Calibrator Catalog and should be better than 0″.1 in accuracy.
[b] *IRAS* 60 μm flux from the pointed observations by Neugebauer et al. 1986.

determination of the source centroid depends somewhat on the S/N of the measurement, and the standard deviation for the 18 objects with S/N > 5 decreases to 5″.5.

For the analysis of the HCG sample, we assume that the statistics obtained from the QSO sample generally apply, including both the intrinsic scatter and the source confusion. One major concern in this assumption is the interplay between the S/N and the position determination. The range of S/N for both the radio QSO and HCG sample are summarized in Table 8. Over $\frac{1}{2}$ (37) of all HCG galaxies are detected with S/N > 20, and the source identification along the average scan direction

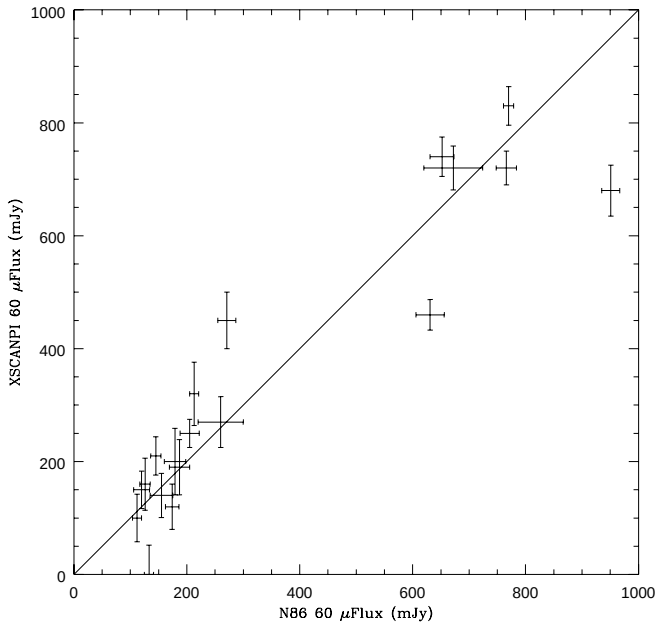

FIG. 10.—Comparison of *IRAS* 60 μm fluxes for the 19 radio-loud QSOs reported by Neugebauer et al. (1986) and by the XSCANPI data. The agreement is rather good, except for a few objects, and the difference can be accounted for by the intrinsic variability of these QSOs.

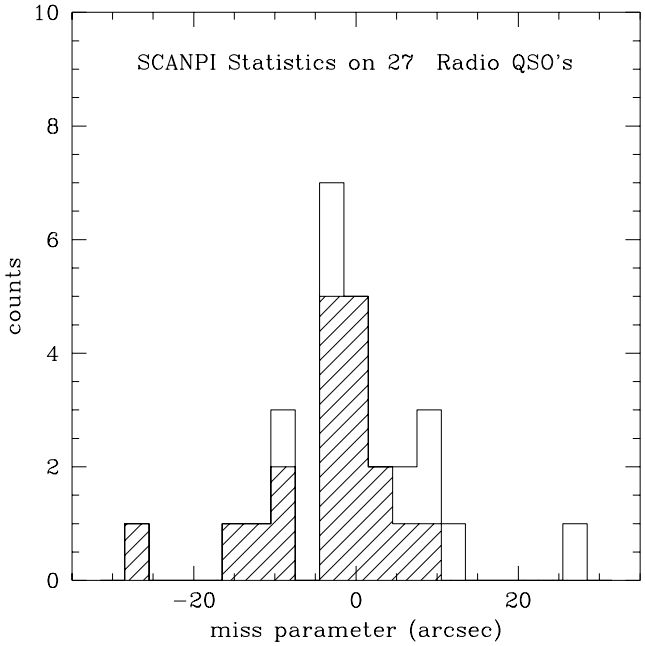

FIG. 11.—Histogram of "miss" parameters for the 27 detected QSOs. Excluding the two outlying sources, which are likely caused by source confusion, the standard deviation of the miss parameter is 6".7 for the entire sample and 5".5 for the 18 objects detected with S/N > 5 (*shaded area*).

TABLE 8

SCANPI DETECTION STATISTICS

	S/N				
SOURCE	Less than 5	5–10	10–15	15–20	Greater than 20
QSO sample	8	11	2	2	4
HCG sample.....	13	12	5	5	37

should be excellent for the HCG sample. For the remaining 35 galaxies, the S/N distribution for detection is similar to that of the QSO sample. Therefore, the standard deviation derived from the analysis of the QSO sample may be safely taken as the upper limit of error in the source identification in the HCG sample.

REFERENCES

Allam, S., Assendorp, R., Longo, G., Braun, M., & Richter, G. 1996, A&AS, 117, 39
Bettoni, D., & Fasano, G. 1993, AJ, 1291, 105
Boselli, A., Casoli, F., & Lequeux, J. 1995, A&A, 110, 521
Boselli, A., Mendes de Oliveira, C., Balkowski, C., Cayatte, V., & Casoli, F. 1996, A&A, 314, 738
Bothum, G. D., Lonsdale, C. J., & Rice, W. 1989, ApJ, 341, 129
Braine, J., & Combes, F. 1993, A&AS, 97, 887
Burstein, D., & Heiles, C. 1984, ApJS, 54, 33
Bushouse, H. A. 1987, ApJ, 320, 49
Combes, F., Prugniel, P., Rampazzo, R., & Sulentic, J. W. 1994, A&A 281, 725
de Vaucouleurs, G., de Vaucouleurs, A., Corwin, H. G., Buta, R. J., Paturel, G., & Fouqué, P. 1991, Third Reference Catalogue of Bright Galaxies (Berlin: Springer) (RC3)
Dultzin-Hacyan, D., Masegosa, J., & Moles, M. 1990, A&A, 238, 28
Dultzin-Hacyan, D., Moles, M., & Masegosa, J. 1988, A&A, 206, 95
Fasano, G., & Bettoni, D. 1994, AJ, 107, 1649
Feigelson, E. D., & Nelson, P. I. 1985, ApJ, 293, 192
Helou, G., Khan, I. R., Malek, L., & Boehmer, L. 1988, ApJS, 68, 151
Hickson, P. 1982, ApJ, 255, 382
———. 1993, ApJ, 29, L1
Hickson, P., Kindl, E., & Auman, J. R. 1989a, ApJS, 70, 687
Hickson, P., Mendes de Oliveira, C., Huchra, J. P., & Palumbo, G. G. C. 1992, ApJ, 399, 353
Hickson, P., Menon, T. K., Palumbo, G. G. C., & Persic, M. 1989b, ApJ, 341, 679
Huchtmeier, W. K. 1997, A&A, 325, 473
Huchtmeier, W. K., & Tammann, G. A. 1992, A&A, 257, 455
Hummel, E. 1981, A&A, 96, 111
Hummel, E., van der Hulst, J. M., Kennicutt, R. C., & Keel, W. C. 1990, A&A, 236, 333
Isobe, T., & Feigelson, E. D. 1990, BAAS, 22, 917
Isobe, T., Feigelson, E. D., & Nelson, P. I. 1986, ApJ, 306, 490
Jog, Ch. J., & Solomon, P. M. 1992, ApJ, 387, 152
Karachentseva, V. E., Lebedev, V. S., & Shcherbanovskij, A. L. 1973, Comm. Special Astrophys. Obs. USSR, 8
Kenney, J. D., & Young, J. S. 1988a, ApJS, 66, 261
———. 1988b, ApJS, 326, 588
Larson, R. B., & Tinsley, B. M. 1978, ApJ, 219, 46
LaValley, M., Isobe, T., & Feigelson, E. D. 1992, in ASP Conf. Ser. 25, Astronomical Data Analysis Software and Systems I, ed. D. M. Worrall, C. Beimesderfer, & J. Barnes (San Francisco: ASP), 245
Lees, J. F., Knapp, G. R., Rupen, M., & Phillips, T. G. 1991, ApJ, 379, 177
Longo, G., Busarello, G., Lorenz, H., Richter, G., & Zagiia, S. 1994, A&A, 282, 418
Marston, A. P. 1988, MNRAS, 231, 333
Mendes de Oliveira, C., & Hickson, P. 1994, ApJ, 427, 689
Menon, T. K. 1995, MNRAS, 274, 845
Menon, T. K., & Hickson, P. 1985, ApJ, 296, 60
Mihos, J. C., & Hernquist, L. 1996, ApJ, 464, 641
Moles, M., del Olmo, A., Perea, J., Masegosa, J., Márquez, I., & Costa, V. 1994, A&A, 285, 404
Neugebauer, G., Soifer, B. T., Miley, G. K., & Clegg, P. E. 1986, ApJ, 308, 815
Perea, J., del Olmo, A., Verdes-Montenegro, L., & Yun, M. S. 1997, ApJ, 490, 166
Rubin, V. C., Hunter, D. A., & Ford, W. K. 1991, ApJS, 76, 153
Sage, L. J. 1993, A&A, 272, 123
Sanders, D. B., Scoville, N. Z., & Soifer, B. T. 1991, ApJ, 370, 158

Sanders, D. B., Scoville, N. Z., Young, J. S., Soifer, B. T., Schloerb, F. P., Rice, W. L., & Danielson, G. E. 1986, ApJ, 305, L45
Savage, B. D., & Mathis, J. S. 1979, ARA&A, 17, 73
Shostak, G. S., Allen, R. J., & Sullivan, W. T., III. 1984, A&A, 139, 15
Solomon, P. M., & Sage, L. J. 1988, ApJ, 334, 613 (SS88)
Stark, A. A., Knapp, G. R., Bally, J., Wilson, R. W., Penzias, A. A., & Rowe, H. B. 1986, ApJ, 310, 660
Sulentic, J. W., & de Mello Rabaça, D. F. 1993, ApJ, 410, 520
Sulentic, J. W., Pietsch, W., & Arp, H. 1995, A&A, 298, 420
Sulentic, J. W., & Rabaça, C. R. 1994, ApJ, 429, 531
Surace, J. A., Mazzarella, J., Soifer, B. T., & Wehrle, A. E. 1993, AJ, 105, 864
Tully, R. B. 1988, Nearby Galaxies Catalog (Cambridge; New York: Cambridge Univ. Press)
Venugopal, V. R. 1995, MNRAS, 277, 455
Verdes-Montenegro, L., del Olmo, A., Perea, J., Athanassoula, E., Márquez, I., & Augarde, R. 1997, A&A, 321, 409
Wiklind, T., Combes, F., & Henkel, C. 1995, A&A, 297, 643
Williams, B. A., McMahon, P. M., & van Gorkom, J. H. 1991, AJ, 101, 1957
Williams, B. A., & Rood, H. J. 1987, ApJS, 63, 265
Williams, B. A., & van Gorkom, J. H. 1988, AJ, 95, 352
Williams, B. A., & van Gorkom, J. H. 1995, in ASP Conf. Ser. 70, Groups of Galaxies, ed. O. G. Richter & K. Borne (San Francisco: ASP), 77
Wolfire, M. G., Hollenbach, D., & Tielens, A. G. G. 1993, ApJ, 402, 195
Xu, C., & Sulentic, J. W. 1991, ApJ, 374, 467
Young, J. S., et al. 1995, ApJS, 98, 219
Young, J. S., & Scoville, N. Z. 1991, ARA&A, 29, 581
Young, J. S., Xie, S., Keney, J. D., & Rice, W. L. 1989, ApJS 70, 699
Yun, M. S., Verdes-Montenegro, L., del Olmo, A., & Perea, J. 1997, ApJ, 475, L21
Zepf, S. E., Whitmore, B. C., & Levison, H. F. 1991, ApJ, 383, 524